WELL-LEVEL MONITORING AT THE CHARLEVOIX GEODYNAMICS OBSERVATORY 1979-1986

by

D.R. Bower

Geophysics Division
Geological Survey of Canada
Energy, Mines and Resources, Canada
Ottawa, Canada

May, 1987

Internal Report
87-2

TABLE OF CONTENTS

1. INTRODUCTION

The Charlevoix Geodynamics Observatory was established in 1976 by the Earth Physics Branch (now the Geophysics Division) to study crustal processes in an intraplate seismic zone. The Charlevoix seismic region, which is one of the most active in eastern North America, is confined to an area 150 km by 40 km centred on the St. Lawrence River approximately 200 km north-east of Quebec City.

Continuous, long-term measurement programs over the years at the observatory have included: surface mounted tilt and strain monitoring (Peters et al, 1981); borehole tilt monitoring (Peters and Beaumont, 1985); special-order levelling measurements (Gagnon et al, 1985) and borehole water level (well level) measurements. Well-level monitoring began in the fall of 1978 when two 68-m (W1 and W2) and one 30-m-deep (W3) vertical boreholes were drilled (Figure 1.1). Current literature at the time (Nur, 1972; Johnson et al, 1974; Scholz and Kranz, 1974) suggested that pore fluids play a major role in the mechanics of earthquakes and, inversely, are a sensitive indicator or diagnostic of this activity. The possible perturbing effect of local ground waters on the sensitive tilt measurements at the site was another factor which made it desirable to monitor pore pressure at depth.

Physical details of the boreholes are shown in Figure 1.1, which also shows the vault where the surface-mounted strain and tilt measurements were made and the adjacent trailer where data logging and communications were centred. The two identical observation holes (W1 and W2) were drilled to provide evidence on the spatial coherence of the pore pressure measurements. The shallow observation hole (W3) was drilled to monitor variations in the water table overlying the partially confined monitored zones. The boreholes designated BT are dedicated, totally cased (and dry) holes in which the borehole tiltmeters were installed.

The meaningful interpretation of the water level data in terms of deformation related events has required borehole tests and the development of theoretical models to determine and remove 'normal' tidal, barometric and hydrological effects.

2. THE HYDROLOGICAL MODEL

2.1 Description

The basic hydrological model adopted is based on one described by Kikkawa (1969). It is assumed that water level variations are known throughout a surficial unconfined water table which overlies a partially confined aquifer in which the pore pressure variations are required to be determined. Water level variations of the water table were calculated using an estimate of infiltration based on the following meteorological data: mean daily temperature (T), rainfall (R) and snowfall (S) for the day, and snow on the ground (H). Infiltration for the day is taken to be 70% of actual precipitation in the case of rain. Daily infiltration by meltwater occurs only so long as there is snow on the ground and is taken to be proportional to the positive difference between the mean temperature for the day and 1.5^{o}. The proportionality constant is taken to be 5 when both rain and snow are measured in the same units. This calculation is implemented by program CONV (Bower et al 1986). Input to program CONV are the daily meteorological data mentioned above and output is used as input to program CONVOL, the function of which is described next.

Changes in water level measured in W1 are assumed to exactly reflect pore pressure variations in the underlying aquifer of the model since hydrological tests (Bower et al, 1986) indicated that well storage was negligible relative to that of the formation and the permeability of the formation was high. Incremental pore pressure in the aquifer was predicted from the model by convolving incremental water level in the upper unconfined layer with the impulse response function of a one-pole low pass filter. Parameters of this filter (two) were determined empirically through fitting to observed well levels in W1 for the year 1981 only. In the absence of precipitation the water level in W1 decays exponentially. This is attributed to evapotranspiration and is estimated by the method of Thornthwaite described by Gray (p 3.56, 1970). It is dependent on the mean air temperature for the month and two parameters given by Gray. A final adjustment was made to the model to compensate for it's lack of memory for precipitation occurring

before the beginning of the calendar year. This adjustment consists simply of an exponential decay with an intial slope equal to that calculated using the model for the previous year. These calculations are implemented by program CONVOL which is listed in Bower et al (1986).

2.3 Results

Plots showing manually observed water level and water level predicted from meteorological data are presented in Figures 2.1 (1979) through 2.7 (1985).

3. BAROMETRIC EFFECT

3.1 Introduction

Atmospheric pressure changes influence the level of water in the well through stress exerted on the surface in the open well and on the solid/fluid components of the surface boundary. The net increase in well water level h, due to an increase in atmospheric pressure p determines the barometric efficiency B.E., defined by:

$$B.E. = -(\rho g h/p) \qquad (3.1\text{-}1)$$

The negative sign is used because an increase in atmospheric pressure causes a decrease in water level. In general the B.E. may or may not be a complex number depending on the elastic and hydrological properties of the medium and the length and diameter of the well bore.

3.2 Analysis

Barometric efficiency was determined using a general purpose cross-spectral analysis program (SPECTRAN) as well as a matrix-based interactive software package (PC-MATLAB, The Mathworks, Inc. 124 Foxwood Rd., Portola Valley, CA., U.S.A.). The episodic nature of the 'noise' in water level records hinders the straightforward

determination of cross correlation by a program such as SPECTRAN. An interactive system with graphics, such as PC-MATLAB, facilitates scanning the data and identifying sections high in barometric energy and relatively free of non-barometric, recharge episodes. However, even with such close attention the B.E. is poorly determined when compared to the determination of the tidal components and there is some suspicion that it may change with time, perhaps with ground water conditions and other parameters.

Program SPECTRAN was used initially to determine that the B.E. was not a function of frequency. PC-Matlab was then used to calculate the covariance between the water level in both W1 and W2 wells and the atmospheric pressure, for data samples selected from the data covering the period 1978 through 1986. Standard linear regression analysis was employed to determine the slope of the line relating pressure to water level and the slope was then expressed in terms of B.E.

3.2.1 Use of PC-MATLAB

Hourly values (n) of atmospheric pressure and water elevation in the well are put in the data vectors p and w respectively. An nx2 matrix M is formed from p (in the first column) and w, with the following PC-MATLAB notation:

```
    M = p;
M(:,2) = w;
```

The covariance matrix is then called with the statement: cov(M), and yields:

$$\mathrm{cov}(M) = \begin{matrix} S_p^2 & S_{pw} \\ S_{pw} & Sw^2 \end{matrix} \qquad (3\text{-}1)$$

where S_p and S_w are the standard deviations of p and w respectively and S_{pw} is the covariance of p and w. The coefficient of linear correlation r is given by:

$$r = S_{pw}/(S_p S_w) \qquad (3\text{-}2)$$

The desired regression line is that of w on p and is given by:

$$w - w' = r\, S_w (p - p'/S_p \qquad (3\text{-}3)$$

where w' and p' are mean values. The slope of this regression line, when p and w are both expressed in the same units, is the Barometric Efficiency. The standard error of the estimate represented by (3) is $S_{y,x}$ where:

$$S_{y,x} = S_y\, (1 - r^2)^{1/2} \qquad (3\text{-}4)$$

3.3 Results

Typical results are illustrated in Figures 3.1 through 3.4. These figures compare the observed water level in W1, after removal of the tides and long-term linear trend, with the predicted barometric effect. Barometric efficiences from .07 to .35 have been determined for particular short sections of data (15-20) days but .22 to .28 is the general range. The striking variations in B.E. at Charlevoix have not been investigated and are not understood. Nevertheless, as will be seen later, the water level corrections based on the computed B.E. improve the tidal analysis, particularly the determination of diurnal constituents, and enhance the interpretation of coseismic water level behaviour.

4. OCEAN TIDE EFFECT

4.1 Calculation

In addition to removing hydrological and barometric effects from the water level data it is necessary to estimate and remove the effect of ocean tides. This effect is generally referred to as load-tide effect to distinguish it from that due to the body tide of the solid earth. The estimation is based on the calculated local elastic strain due to the surface force exerted by ocean tides as well as the body forces

exerted by both the ocean waters and the displaced masses of the earth. The calculation requires ocean tide maps and assumptions on the physical properties of the earth as a function of depth. The assumptions adopted are those incorporated in a Green's function developed by Farrel (1972) for this purpose and which reflect a Gutenberg-Bullen model earth. The convolution was carried out by Peters (1985, personal communication) using a version of program GLOBL (Bower, 1971) with local ocean tide detail covering the east coast and the St. Lawrence River. The results of this calculation are expressed as complex strain tensors for both the M_2 and O_1 constituents. The strain due to the theoretical body tide was also calculated (Program STRESS, in Bower et al (1986)) for both the M_2 and O_1 constituents. The sum of load-tide and body-tide tensors yields the predicted total strain of the model earth. These data are reproduced in Table 4.0

4.2 Results

Further assumptions are required before the predicted total strain tensor can be related to the observed well-level tide. The predicted strain is based on the whole-body deformation of the model earth and it is evident that on a local scale the actual tidal strain of the surface will differ from point to point because of cracks and other heterogenities. Nevertheless the assumption is made here that on a boundary enclosing the region in which the borehole is embedded, and located within tens of metres of the borehole, the strain is that of the assumed tidal strain. The well-level tide then is predicted on the basis that the enclosed region is either: (a) homogeneous and isotropic, with given porosity , hydraulic conductivity and elasticity or (b) contains a single, planar fracture which intersects the borehole and is of given aperture and compressibility. The considerations relevant to these two models are discussed by Bower et. al. (1986a) and the single fracture model is developed in detail by Bower (1983).

To facilitate a comparison of observations and predictions the predicted data is presented in the form shown in Tables 4.1 and 4.2. The principal tabular data are the predicted linear tidal strain amplitude and phase in the vector direction given by azimuth and dip. Also shown is the stress amplitude and phase in this same direction,

calculated on the assumption of the elastic parameters indicated. The amplitude and phase of the tidal pore pressure and the volume dilatation, both calculated on the assumption of a homogeneous medium, are shown in Table 4.2.

These results are developed from the basic strain tensors in program TENSOR, which is listed in Bower et al (1986). An interpretation of the results is given later.

5. OBSERVED WELL-LEVEL TIDE

5.1 Results

A summary of the results of tidal analysis of data from both wells W1 and W2 is presented in Table 5.1. If the wells are embedded in a porous medium which is elastically homogeneous and isotropic to the far field these data should reflect the volumetric strain predictions presented in Table 4.2. In particular, the predicted and observed phase and amplitude ratio data should be similar since these quantities are relatively independent of elastic and hydrological parameters which are generally unknown. (Hydrological tests show negligible draining effects due to the presence of the borehole and thus negligible effect on the tidal phases is indicated). In fact, the observed amplitude ratio (2.5 to 2.75) is much larger than that predicted (1.75) and the observed O_1 phase is significantly more positive than predicted. Comparison with the predicted linear strain (Table 4.1) on the other hand suggests the predominant influence of (approximately) north-east linear strain.

These observations are illustrated in Figures 5.1, 5.2 and 5.3. While it can be seen that the M_2 phase alone does not distinguish between the volumetric and linear strain models the O_1 phase and the ratio of the amplitudes clearly favour the linear strain model. A plausible and interesting explanation for this is that the far-field tidal strain is decoupled from the region in which the borehole is drilled by one or both of the Gouffre and St. Laurent faults. These are steeply dipping faults which strike north 30°-50° east (Anglin, 1984) and intersect the surface 5km northwest and southeast of the Charlevoix site respectively. The observed well tide, and the pore

pressure which it reflects, appears to respond mainly to that component of tidal strain roughly parallel to these faults.

Anglin (1984) points out that the Gouffre fault is the major northwest boundary of seismic activity. This and the tidal decoupling revealed above suggest an active, relatively weak zone (or a parallel set of such zones) which will be of some significance in the search for earthquake precursors or the interpretation of coseismic well-level changes. For example, there is some indication in the data (see below) that the degree of tidal decoupling may not be constant and if this is the case, changes, determined from well-level observations, may reflect changes in pore pressure conditions on one or more north-east striking fault surfaces.

5.2 Change of Tidal Response with Time

Figure 5.4 illustrates the variation with respect to time of the observed M_2 tidal amplitude and phase from 1981 until 1986. Although the variation from analysis to analysis is large there appears to be a systematic trend over time in both amplitude and phase as well as coherent short term variations. In fact, a regression analysis of phase on amplitude yields a correlation coefficient of -0.61 and the following equation relating phase to amplitude:

$$F_2 \text{ (phase in deg.)} = -48.8-31.0*h_2 \text{ (amplitude in cm.)} \quad (5\text{-}1)$$

This is a significant if not a marked correlation that may have important implications to the interpretation of the coseismic response of the well level. Possible explanations considered for the change with time of these observables are as follows:

1. Change with time of the well-level measuring transducer or the calibration technique.
2. Change with time of the hydrological properties of the borehole/aquifer connection, perhaps due to accumulation of pore filling materials near the borehole wall.
3. A change in the local elastic parameters, preserving isotropy.

4. Change in fracture permeabilities due to a systematic change in the water table, possibly related to drilling on the site in 1978 and 1981, with the effect of decreasing the influence of some intersected fractures and increasing the influence of others.
5. Local or regional anistropy related to changing conditions on one or more distant faults.

The first explanation can be eliminated because: (a) the phase measurement is independent of transducer calibration; (b) many transducers were used over the six years of data; (c) the calibration ultimately is related to hand measurements made with a tape at the well head, usually at least once per week.

The second explanation would lead to systematic changes in amplitude and phase (or amplitude alone) with relative polarity opposite to that observed. That is, decreased permeability would result in a decreased tidal amplitude and either no change in phase or an increased phase lag. In fact we observe a decreased tidal amplitude and a decrease in phase lag. Further, hydrological tests have shown that the well level tide observed is not affected by the presence of the borehole, either with respect to amplitude or phase.

The third explanation to apply would require only a change in amplitude but not a change in phase since both body and load tides would be affected equally.

The fourth and fifth explanations can not be distinguished from one another on the basis of tidal observations. A simplified model to evaluate the fifth explanation is discussed below.

The basis for this model is the extreme difference between an isotropic elastic medium, assumed to be the case at the beginning of 1981, and an anistropic medium with zero tidal stress at right angles to some azimuth AZ to be determined, in 1986. This model is suggested by the known fault structure in the area (Anglin, 1984) and by the results discussed in section 5.1 above. For this model predictions calculated for all azimuths are reproduced in Table 5.2. The observed amplitude and phase at the beginning and the end of the data series are taken, from Figure 5.4, to be .54 cm, -60.0^{o} and .45 cm, -51.0^{o} respectively. The ratio of these two vectors is .83, $+9.8^{o}$. Comparing this observed ratio with that predicted by the model reveals a best match in the

region of AZ = 070°. Thus the observations of the M_2 constituent are consistent with gradual decoupling of the well locality from stresses in this azimuth.

This conclusion, which is based on the long-term change in the M_2 well tide, lends some support to the conclusion reached in section 5.2 regarding the decoupling of tidal strain in the direction perpendicular to the azimuth of 40°-70° and the possible connection with the nearby Gouffre fault. The latter conclusion was based on the average M_2 and O_1 well tides over the whole interval 1981 to 1986. The present conclusion, taking into account only the coherent, systematic changes with time of the M_2 constituent, suggests that both observations may be consistent with progressive decoupling of tidal strains in the azimuth of 160° (ie. AZ=70°).

Ideally we should apply the method employed in section 5.2 to shorter sections of data to demonstrate a truly consistent picture of this behaviour but the large experimental error in the determination of the O_1 amplitude and phase from 1-month-long data sets prevents this. What can be said however is that over the period 1981-1986 the O_1 phase changes by approximately +40° and the amplitude decreases by a factor of 0.88. The direction of these changes is consistent with that of the model data in Table 5.2 but the magnitude is decidedly too large in one case (phase) and too small in the other.

6. COSEISMIC AND SHORT-TERM POSTSEISMIC OBSERVATIONS

6.1 Introduction

In this section I define coseismic conditions to include short-term postseismic conditions, where short-term refers to a few days.

Although the principal objective of the water-level monitoring was to find earthquake precursors, expected to be in the form of sudden dilatancy effects, it gradually became apparent that we should instead concentrate on identifying and accounting for coseismic water-level effects. We realized that preseismic effects were certain to be much smaller, probably not discernible at all for most Charlevoix earthquakes, and liable to occur as far in advance of the earthquake as

a few months. Understanding the coseismic water-level response on the other hand, for earthquakes with known source parameters, could provide a basis for searching for and interpreting precursory strain/stress phenomena.

6.2 Results

Table 6.1 lists all Charlevoix earthquakes of magnitude 3.0 or greater which occurred during the period 1976 to February 1, 1986. A well defined coseismic change in well level was observed in only the four cases noted in the table. For each of these cases the observations were systematically treated to remove tides, barometric effects (except for the 1983 event when barometric data was not available) and long term linear or exponential trends. The well level predicted on the basis of the hydrological model and meteorological data is not quite definitive enough to justify subtracting it from the observations. Instead, it is compared visually with the corrected observed water level for the purpose of revealing whether a particular observed behaviour is or is not consistent with hydrological conditions.

The four coseismic cases are illustrated in Figures 6.1 through 6.8. In most cases the observed water level has been corrected for earth tides, barometric effect and a long term exponential decay. The fit of a long term exponential decay is illustrated in the 1979 case in Figure 6.3. Figure 6.1 compares the well level in the weeks about this earthquake with the water level predicted by the hydrological model. It is possible to conclude from this comparison that the well level in the period day 230 to day 240 should not be influenced by recharge. This period is shown in detail in Figure 6.2. The exponential drop in water level coincident with the earthquake, followed by a slower exponential recovery is more or less characteristic of all four cases. The rise in observed water level at day 197 is inconsistent with the behaviour predicted by the hydrological model and might indicate that the model (including the meteorological input) is faulty or it might reflect precursory dilatancy in the region near the location of the eventual earthquake.

The detail about the 1982 earthquake, shown in Figure 6.4, suggests the characteristic fall and subsequent recovery of water level referred

to above. However, comparison with the predicted water level in Figure 6.5 shows that the 'recovery' is probably mainly due to natural recharge. The intial fall in water level on the other hand is probably not appreciably distorted by natural discharge.

Barometric pressure was not available near the time of the 1983 earthquake so an additional uncertainty is introduced to the interpretation of the coseismic water level change reproduced in Figures 6.6 and 6.7. The rise in water level beginning near day 145, before the earthquake, however appears to be anomolous. There is a suggestion of a recovery period after the earthquake but this cannot be determined in the presence of an apparent superimposed recharge episode.

Predictions based on the hydrological model were not available for reduction of the well level data about the time of the 1986 earthquake shown in Figure 6.8. This figure shows both the edited and the unedited water level data and illustrates the large barometric pressure effect present in the latter. Since there was no reported rainfall or melting up to at least day 17 the edited data is probably undistorted up to this date. The rise in water level beginning on day 8 appears to be anomolous.

6.3 Discussion.

Only the well level observation for the 1979 earthquake has so far been compared with a calculated residual strain field. According to Hasegawa (private communication, 1986), and assuming a uniform crust and no unconsolidated surface sediments, the 1979 event should have produced a volume dilatation of 0.1×10^{-8} at the Charlevoix site. This is an order of magnitude less than the far-field M_2 tidal volumetric strain yet the observed coseismic well level change was greater than the M_2 well level change by a factor of 6. This result contrasts with that of Avon et al (1985) who found good agreement between well-level coseismic volumetric strain and volumetric strain calculated from elastic dislocation theory applied to local earthquakes on the San Andreas fault.

Apart from the magnitude problem an attempt was made to account for the shape of the coseismic and postseismic water level changes through modelling. The borehole was assumed to be embedded in a saturated

infinite half space of given hydraulic diffusivity which is suddenly dilated below a given depth. The diffusivity and the depth were parameters to be determined. This model is suggested by the observations because it results in an initial exponential fall in water level followed by a slower exponential recovery due to recharge of the dilated half space from the water table. For the 1979 event the best fitting model depth was found to be just equal to the depth of the borehole and the diffusivity was .028 m^2/sec. However, these model parameters turned out to be inconsistent with estimates of the same parameters based on the combination of observed well tide response and the hydrological tests. In addition, it was found that the model results were consistent with the coseismic observations only for a very narrow range of depths near the borehole depth. This was suspicious and, together with the hydrological tests and the earth tide response, suggested that the well level response with time was not in fact distorted by well/aquifer dynamics and did accurately reflect the behaviour with time of volume strain about the well. This is a significant conclusion and leads to speculation on possible explanations for both the shape and the magnitude of the response consistent with the dilatancy theory of earthquakes. This is developed further in the next section.

6.4 Possible Dilatancy Effect

According to the dilatancy theory of earthquakes an earthquake is preceded by a period of stress build-up during which wide spread microcracking occurs, at stress levels in the order of one half of breaking strength, resulting in the creation of a dilatant 'zone'. Pore pressure within the dilatant zone drops, strengthening the rock through a process described by Hubbert and Rubey (1959) as 'locking the rock in place'. Stress continues to increase while pore fluid diffuses into the new dilatancy from surrounding regions. Depending on the diffusivity, the dilatant zone size and the rate of stress increase, the occurrence of dilatancy postpones the earthquake. That is, pore pressure eventually rises and strength falls to the point where the ambient stress can not be supported and an earthquake occurs.

Coincident with the earthquake the stress which created and supported

the dilatancy is relieved and the dilatancy tends to close, increasing the pore pressure. Large pressure gradients are created near the boundary of the dilatant zone and draining to the surrounding region occurs. As draining progresses dilatancy is lost at a decreasing rate from the boundary inward. A quantitative estimate of the effect of this dilatancy change on volume strain at the observatory can be made based on the analysis of Hagiwara (1977) of the dilatation produced by an expanding or contracting sphere. According to Hagiwara the dilatation Δ at the point of observation is:

$$\frac{\Delta}{\Delta^\circ} = \frac{4a^3 (R^2 - 2D^2)}{3(\lambda+\mu)(R^2+D^2)^{5/2}}$$

where Δ° is the dilatation at the source, a is the radius of the dilated zone, D is the depth to the centre of the sphere and λ and μ are elastic constants. This equation was solved for Δ° for the four earthquakes for which water level changes were observed and the results are reproduced in Table 6.2. The volume strain at the well was inferred from the short-term postseismic change in well level using the observed relation between level change and tidal volume strain.

7. CONCLUSIONS

The utility of well-level monitoring is critically dependent on the degree to which barometric and meteorologically induced effects can be removed from the observations. This impacts both on the problem of distinguishing precursory deformation effects and on the problem of using the well tide to calibrate the well-aquifer system for it's response to changes in local and far-field strain and stress. Considerable success has been achieved in the Charlevoix study in modelling and removing these extraneous effects but the large experimental error characterizing measurements of the diurnal well tide remains a serious problem.

Current well-level tide measurements of both semidiurnal and diurnal constituents indicate an anomolously large contribution from tidal strain in the azimuth of 70°. M_2 tidal measurements over the period 1981-1986 reveal a systematic change with time which can be explained as

an increasing response in the azimuth of 070° (±30°) to tidal stress. These independent determinations suggest mechanical changes in one or more of the north-east trending faults described by Anglin (1984).

Coseismic and short-term postseismic effects on well level were observed for only 4 earthquakes during the period 1978-1986 but showed, more or less, the same general character in each case: a rapid exponential decay in level followed by a slower exponential recovery. This observation does not seem to be affected by the dynamic response of the well/aquifer system and probably reflects elastic strain changes much closer to the earthquake. Calculations based on a simple dilatancy model indicate that the strain changes may represent the discharge of excess pore fluids from the outer regions of a relaxing dilatant zone about the earthquake. This theory is novel and requires further investigation using a mechanical model incorporating full coupling between elastic deformation and fluid flow.

ACKNOWLEDGEMENTS

I gratefully acknowledge the dedicated support and collaboration of the other members of the Charlevoix Observatory Group, supervised by Tony Lambert and including Jacques Labrecque and Evelyn Mitchell. I am grateful too for the excellent technical support provided by the Instrumentation Section under the supervision of Herb Valliant and including Nicholas Courtier, Rick Beach and Cary Gagnon.

REFERENCES

Anglin, F.M., Seismicity and Faulting in the Charlevoix Zone of the St. Lawrence valley. B.S.S.A., 74, 595-603, 1984.

Bower, D.R., and Heaton K.C., Response of an Aquifer Near Ottawa to Tidal Forcing and the Alaskan earthquake of 1964, Can. J. Earth Sci., 15(3), 331-340, 1978.

Bower, D.R., Lambert A., Labrecque J.J. and Mitchell E.M., Inventory of Data from the Charlevoix Geodynamics Observatory. Internal Report of the Geophysics Division of the Geological Survey of Canada. 1986.

Bower, D.R., Davison, C.C. and E.Kozak, Tidal Observations in Piezometers at the Site of Canada's Underground Research Laboratory, A.E.C.L. Internal Report, Atomic Energy of Canada, Pinawa, Manitoba, R0E 1L0

Farrell, W.E., Deformation of the Earth by Surface Loads. Rev. Geophys. Space Phys., 10, 761-797, 1972.

Gagnon, P., Jobin, J., Sanchez, R. and G. Arancibia, Etude des Resultats des Mesures Mensuelles de Nivellement a l'Observatoire Geophysique de Charlevoix pour la periode 1978-1984. Faculte de Foresterie et de Geodesie, Universite Laval, Quebec, Canada. 1985.

Gray, D.M., Handbook on the Principles of Hydrology, The Water Information Center, Inc., Water Research Building, Manhasset Isle., Port Washington, N.Y. 11050. 1970.

Johnson, A.G., Kovach R.L., and Nur A., Fluid Pressure Variations and Fault Creep in Central California. Tectonophysics, 23, 257-266, 1974.

Kikkawa, K., A Method to Analyse the Effect of Precipitation on the Ground Water Stream. Special Contributions, Geophysical Institute, Kyoto University, No. 9., 1-14, 1969.

Nur, A., Dilatancy, Pore Fluids, and Premonitory Variations in t_s/t_p Travel Times, Bull. Seismol. Soc. Amer., 62, 1217-1223, 1972.

Peters, J.A., Bower, D.R. and A.Lambert. Tidal Tilt Response at Charlevoix, Quebec. Proceedings of the 9th International Symposium on Earth Tides, New York, August 12-22, pp 59-68,1981.

Peters, J.A. and Beaumont, C., Borehole Tilt Measurements From Charlevoix, Quebec. J.Geophys.Res., 90, 12791-12806, 1985.

Scholz, C.H. and Kranz, R., Notes on Dilatancy Recovery, J. Geophys. Res., 79, 2132-2135, 1974.

THEORETICAL BODY STRAIN TENSOR FOR M2

1.41	.0°	4.71	.0°	.0	.0°
4.71	-91.0°	11.29	.0°	.0	.0°
.0	.0°	.0	.0°	3.24	180.0°

THEORETICAL BODY STRAIN TENSOR FOR 01

7.27	.0°	1.88	90.0°	.0	.0°
1.88	90.0°	4.50	.0°	.0	.0°
.0	.0°	.0	.0°	2.94	180.0°

OCEAN LOAD STRAIN TENSOR FOR M2

11.85	-52.6°	2.88	-9.7°	.0	.0°
2.88	-9.7°	13.09	-155.7°	.0	.0°
.0	.0°	.0	.0°	3.88	72.3°

OCEAN LOAD STRAIN TENSOR FOR 01

1.29	185.0°	.26	123.0°	.0	.0°
.26	123.0°	1.36	132.0°	.0	.0°
.0	.0°	.0	.0°	.59	-22.0°

TABLE 4.0 Strain tensors used to predict total strain in any direction. Complex strain components are in nano-strain and phase (degrees relative to tide generating potential). Principal axes 1, 2 and 3 are east, north and down. (Load strains from Peters, per. comm., 1985)

STRESS AND STRAIN IN A GIVEN DIRECTION DUE TO BODY AND LOAD TIDES

Az	Dip	Strain(O1)		Stress(O1)		Strain(M2)		Stress(M2)		Ratios(M2/O1) Str.	Stress
		amp	phase	amp	phase	amp	phase	amp	phase	amp	phase
0	0	3.73	15.7	4.18	10.6	5.42	-96.8	6.40	-78.1	1.45	1.53
10	0	3.99	25.1	4.25	13.0	7.31	-85.4	7.06	-75.6	1.83	1.66
20	0	4.39	30.5	4.38	14.3	9.46	-76.5	7.88	-71.9	2.15	1.80
30	0	4.80	32.1	4.56	14.4	11.62	-69.6	8.78	-67.7	2.42	1.93
40	0	5.15	30.5	4.76	13.3	13.52	-64.1	9.68	-63.7	2.62	2.03
50	0	5.42	26.5	4.97	11.4	14.89	-59.8	10.46	-60.2	2.75	2.10
60	0	5.63	20.7	5.17	9.0	15.55	-56.1	11.03	-57.2	2.76	2.13
70	0	5.78	13.7	5.33	6.4	15.40	-52.9	11.31	-54.9	2.66	2.12
80	0	5.90	6.2	5.44	3.7	14.44	-50.0	11.24	-53.2	2.45	2.07
90	0	5.99	-1.1	5.48	1.4	12.76	-47.6	10.82	-52.3	2.13	1.97
100	0	6.01	-7.6	5.45	-0.6	10.54	-45.5	10.10	-52.2	1.75	1.85
110	0	5.95	-12.9	5.35	-1.9	8.03	-44.2	9.17	-53.2	1.35	1.71
120	0	5.75	-16.7	5.18	-2.5	5.53	-45.0	8.13	-55.5	0.96	1.57
130	0	5.41	-18.5	4.96	-2.3	3.35	-51.8	7.15	-59.3	0.62	1.44
140	0	4.96	-17.8	4.72	-1.0	1.99	-76.4	6.37	-64.6	0.40	1.35
150	0	4.45	-14.1	4.49	1.2	2.03	-110.7	5.89	-70.5	0.46	1.31
160	0	3.99	-6.8	4.31	4.1	2.85	-117.8	5.76	-75.5	0.71	1.34
170	0	3.72	4.0	4.20	7.5	3.95	-109.3	5.95	-78.2	1.06	1.42
180	0	3.73	15.7	4.18	10.6	5.42	-96.8	6.40	-78.1	1.45	1.53
0	15	3.32	16.2	3.90	10.6	4.83	-98.7	5.97	-78.1	1.45	1.53
10	15	3.57	26.0	3.96	13.0	6.56	-86.5	6.59	-75.6	1.84	1.66
20	15	3.95	31.5	4.09	14.3	8.55	-77.0	7.35	-71.9	2.16	1.80
30	15	4.33	33.0	4.25	14.4	10.57	-69.8	8.19	-67.7	2.44	1.93
40	15	4.66	31.3	4.45	13.3	12.33	-64.2	9.03	-63.7	2.65	2.03
50	15	4.91	27.1	4.64	11.4	13.61	-59.7	9.76	-60.2	2.77	2.10
60	15	5.09	21.1	4.82	9.0	14.23	-56.0	10.30	-57.2	2.80	2.14
70	15	5.23	13.9	4.97	6.4	14.09	-52.7	10.55	-54.9	2.69	2.12
80	15	5.34	6.2	5.07	3.7	13.19	-49.8	10.49	-53.2	2.47	2.07
90	15	5.43	-1.3	5.11	1.4	11.63	-47.2	10.10	-52.3	2.14	1.98
100	15	5.45	-8.0	5.09	-0.6	9.56	-45.0	9.43	-52.2	1.75	1.85
110	15	5.40	-13.5	4.99	-1.9	7.22	-43.6	8.55	-53.2	1.34	1.71
120	15	5.22	-17.3	4.83	-2.5	4.88	-44.1	7.59	-55.5	0.93	1.57
130	15	4.90	-19.2	4.63	-2.3	2.85	-50.9	6.67	-59.3	0.58	1.44
140	15	4.48	-18.7	4.40	-1.0	1.59	-79.2	5.94	-64.6	0.35	1.35
150	15	4.00	-14.9	4.19	1.2	1.72	-117.9	5.49	-70.5	0.43	1.31
160	15	3.56	-7.3	4.02	4.1	2.51	-123.2	5.37	-75.5	0.70	1.34
170	15	3.31	3.9	3.92	7.5	3.51	-112.7	5.55	-78.2	1.06	1.42
180	15	3.32	16.2	3.90	10.6	4.83	-98.7	5.97	-78.1	1.45	1.53
0	30	2.21	18.5	3.14	10.6	3.27	-107.7	4.80	-78.0	1.48	1.53
10	30	2.44	29.9	3.19	13.0	4.54	-91.0	5.29	-75.6	1.86	1.66

TABLE 4.1a Stress in cm of water equivalent, strain in nanostrain, phase in deg. ($\lambda = \mu = 28$ GPa)

STRESS AND STRAIN IN A GIVEN DIRECTION DUE TO BODY AND LOAD TIDES

Az	Dip	Strain(O1)		Stress(O1)		Strain(M2)		Stress(M2)		Ratios(M2/O1) Str.	Stress
		amp	phase	amp	phase	amp	phase	amp	phase	amp	phase
20	30	2.76	35.8	3.29	14.3	6.08	-79.1	5.91	-71.9	2.20	1.80
30	30	3.07	37.1	3.42	14.4	7.67	-70.7	6.59	-67.7	2.50	1.93
40	30	3.33	34.9	3.57	13.3	9.08	-64.5	7.26	-63.7	2.73	2.03
50	30	3.51	30.0	3.73	11.4	10.11	-59.6	7.85	-60.2	2.88	2.10
60	30	3.64	23.2	3.87	9.0	10.61	-55.6	8.28	-57.2	2.91	2.14
70	30	3.74	15.0	4.00	6.4	10.51	-52.1	8.48	-54.9	2.81	2.12
80	30	3.82	6.4	4.08	3.7	9.79	-48.9	8.43	-53.2	2.56	2.07
90	30	3.89	-2.1	4.11	1.4	8.54	-45.9	8.12	-52.3	2.19	1.98
100	30	3.93	-9.6	4.09	-0.6	6.89	-43.2	7.58	-52.2	1.75	1.85
110	30	3.89	-15.7	4.01	-1.9	5.02	-40.8	6.87	-53.2	1.29	1.71
120	30	3.76	-20.1	3.88	-2.5	3.14	-39.7	6.10	-55.5	0.83	1.57
130	30	3.52	-22.4	3.72	-2.3	1.48	-45.3	5.36	-59.3	0.42	1.44
140	30	3.17	-22.1	3.54	-1.0	0.55	-107.3	4.77	-64.6	0.17	1.35
150	30	2.78	-18.3	3.37	1.2	1.16	-154.7	4.41	-70.5	0.42	1.31
160	30	2.41	-9.7	3.23	4.1	1.79	-147.5	4.32	-75.5	0.74	1.34
170	30	2.19	3.6	3.15	7.5	2.40	-128.5	4.46	-78.2	1.10	1.42
180	30	2.21	18.5	3.14	10.6	3.27	-107.7	4.80	-78.0	1.48	1.53
0	45	0.72	33.4	2.09	10.6	1.59	-147.9	3.20	-78.0	2.21	1.53
10	45	0.96	50.3	2.12	13.0	1.94	-112.4	3.53	-75.6	2.02	1.66
20	45	1.22	55.3	2.19	14.3	2.75	-88.4	3.94	-71.9	2.25	1.80
30	45	1.43	54.2	2.28	14.4	3.73	-74.5	4.39	-67.7	2.61	1.93
40	45	1.57	49.4	2.38	13.3	4.65	-65.6	4.84	-63.7	2.96	2.03
50	45	1.65	41.7	2.49	11.4	5.33	-59.3	5.23	-60.2	3.23	2.10
60	45	1.68	31.6	2.58	9.0	5.67	-54.3	5.52	-57.2	3.37	2.14
70	45	1.71	19.6	2.66	6.4	5.61	-49.9	5.65	-54.9	3.28	2.12
80	45	1.75	6.9	2.72	3.7	5.16	-45.6	5.62	-53.2	2.95	2.07
90	45	1.80	-5.3	2.74	1.4	4.35	-41.1	5.41	-52.3	2.42	1.97
100	45	1.86	-15.9	2.73	-0.6	3.28	-35.6	5.05	-52.2	1.76	1.85
110	45	1.87	-24.5	2.67	-1.9	2.08	-27.3	4.58	-53.2	1.11	1.72
120	45	1.82	-30.9	2.59	-2.5	0.93	-6.5	4.07	-55.5	0.51	1.57
130	45	1.68	-35.2	2.48	-2.3	0.53	89.3	3.58	-59.3	0.32	1.44
140	45	1.45	-36.8	2.36	-1.0	1.19	132.1	3.18	-64.6	0.82	1.35
150	45	1.16	-34.3	2.24	1.2	1.65	147.0	2.94	-70.5	1.42	1.31
160	45	0.86	-23.7	2.15	4.1	1.79	160.8	2.88	-75.5	2.08	1.34
170	45	0.66	1.7	2.10	7.5	1.68	-179.4	2.97	-78.2	2.55	1.41
180	45	0.72	33.4	2.09	10.6	1.59	-147.9	3.20	-78.0	2.21	1.53
0	60	0.90	174.5	1.05	10.6	2.22	140.1	1.60	-78.0	2.47	1.52
10	60	0.93	163.8	1.06	13.0	1.69	145.8	1.76	-75.6	1.82	1.66
20	60	0.94	155.3	1.10	14.3	1.10	154.5	1.97	-71.8	1.17	1.79
30	60	0.91	148.8	1.14	14.4	0.53	174.7	2.20	-67.7	0.58	1.93

TABLE 4.1b Stress in cm of water equivalent, strain in nanostrain, phase in deg. ($\lambda = \mu = 28$ GPa)

STRESS AND STRAIN IN A GIVEN DIRECTION DUE TO BODY AND LOAD TIDES

Az	Dip	Strain(O1)		Stress(O1)		Strain(M2)		Stress(M2)		Ratios(M2/O1) Str.	Stress
		amp	phase	amp	phase	amp	phase	amp	phase	amp	phase
40	60	0.84	144.5	1.19	13.3	0.28	-104.7	2.42	-63.7	0.33	2.03
50	60	0.73	142.9	1.24	11.4	0.55	-53.3	2.62	-60.1	0.75	2.11
60	60	0.58	145.3	1.29	9.0	0.77	-35.9	2.76	-57.2	1.33	2.14
70	60	0.43	155.7	1.33	6.4	0.83	-20.9	2.83	-54.9	1.93	2.13
80	60	0.33	-178.9	1.36	3.7	0.77	0.4	2.81	-53.2	2.33	2.07
90	60	0.36	-146.9	1.37	1.4	0.74	34.6	2.71	-52.3	2.06	1.98
100	60	0.48	-129.8	1.36	-0.6	0.94	71.3	2.53	-52.2	1.96	1.86
110	60	0.61	-124.7	1.34	-1.9	1.38	94.4	2.29	-53.2	2.26	1.71
120	60	0.71	-125.8	1.29	-2.5	1.88	107.5	2.03	-55.5	2.65	1.57
130	60	0.78	-130.6	1.24	-2.3	2.35	115.9	1.79	-59.3	3.01	1.44
140	60	0.82	-138.4	1.18	-1.0	2.70	122.0	1.59	-64.5	3.29	1.35
150	60	0.84	-148.6	1.12	1.2	2.87	126.9	1.47	-70.5	3.42	1.31
160	60	0.85	-160.6	1.08	4.1	2.85	131.2	1.44	-75.5	3.35	1.33
170	60	0.87	-173.4	1.05	7.5	2.62	135.5	1.49	-78.2	3.01	1.42
180	60	0.90	174.5	1.05	10.6	2.22	140.1	1.60	-78.0	2.47	1.52
0	75	2.00	-176.0	0.28	10.6	3.66	122.5	0.43	-77.9	1.83	1.54
10	75	1.99	-177.3	0.28	13.0	3.51	122.4	0.47	-75.5	1.76	1.68
20	75	1.98	-178.4	0.29	14.3	3.34	122.0	0.53	-71.8	1.69	1.83
30	75	1.96	-179.0	0.31	14.3	3.18	121.2	0.59	-67.6	1.62	1.90
40	75	1.94	-179.1	0.32	13.3	3.04	120.1	0.65	-63.6	1.57	2.03
50	75	1.91	-178.7	0.33	11.4	2.95	118.7	0.70	-60.1	1.54	2.12
60	75	1.88	-177.8	0.35	9.0	2.91	117.4	0.74	-57.1	1.55	2.11
70	75	1.86	-176.5	0.36	6.3	2.93	116.3	0.76	-54.8	1.58	2.11
80	75	1.85	-174.9	0.36	3.7	3.00	115.7	0.75	-53.2	1.62	2.08
90	75	1.84	-173.3	0.37	1.3	3.12	115.5	0.73	-52.3	1.70	1.97
100	75	1.85	-171.9	0.37	-0.6	3.27	115.8	0.68	-52.2	1.77	1.84
110	75	1.87	-170.9	0.36	-1.9	3.44	116.6	0.61	-53.1	1.84	1.69
120	75	1.89	-170.4	0.35	-2.5	3.59	117.5	0.54	-55.4	1.90	1.54
130	75	1.92	-170.3	0.33	-2.3	3.73	118.6	0.48	-59.2	1.94	1.45
140	75	1.94	-170.9	0.32	-1.0	3.82	119.7	0.43	-64.4	1.97	1.34
150	75	1.96	-171.8	0.30	1.2	3.86	120.7	0.39	-70.4	1.97	1.30
160	75	1.98	-173.1	0.29	4.1	3.85	121.5	0.39	-75.4	1.94	1.34
170	75	1.99	-174.6	0.28	7.5	3.78	122.1	0.40	-78.1	1.90	1.43
180	75	2.00	-176.0	0.28	10.6	3.66	122.5	0.43	-77.9	1.83	1.54
0	90	2.40	-174.7	0.00	0.0	4.23	119.1	0.00	0.0	1.76	0.00
10	90	2.40	-174.7	0.00	0.0	4.23	119.1	0.00	0.0	1.76	0.00
20	90	2.40	-174.7	0.00	0.0	4.23	119.1	0.00	0.0	1.76	0.00
30	90	2.40	-174.7	0.00	0.0	4.23	119.1	0.00	0.0	1.76	0.00
40	90	2.40	-174.7	0.00	0.0	4.23	119.1	0.00	0.0	1.76	0.00
50	90	2.40	-174.7	0.00	0.0	4.23	119.1	0.00	0.0	1.76	0.00

TABLE 4.1c Stress in cm of water equivalent, strain in nanostrain, phase in deg. ($\lambda = \mu = 28$ GPa)

STRESS AND STRAIN IN A GIVEN DIRECTION DUE TO BODY AND LOAD TIDES

Az	Dip	Strain(O1)		Stress(O1)		Strain(M2)		Stress(M2)		Ratios(M2/O1) Str.	Stress
		amp	phase	amp	phase	amp	phase	amp	phase	amp	phase
60	90	2.40	-174.7	0.00	0.0	4.23	119.1	0.00	0.0	1.76	0.00
70	90	2.40	-174.7	0.00	0.0	4.23	119.1	0.00	0.0	1.76	0.00
80	90	2.40	-174.7	0.00	0.0	4.23	119.1	0.00	0.0	1.76	0.00
90	90	2.40	-174.7	0.00	0.0	4.23	119.1	0.00	0.0	1.76	0.00
100	90	2.40	-174.7	0.00	0.0	4.23	119.1	0.00	0.0	1.76	0.00
110	90	2.40	-174.7	0.00	0.0	4.23	119.1	0.00	0.0	1.76	0.00
120	90	2.40	-174.7	0.00	0.0	4.23	119.1	0.00	0.0	1.76	0.00
130	90	2.40	-174.7	0.00	0.0	4.23	119.1	0.00	0.0	1.76	0.00
140	90	2.40	-174.7	0.00	0.0	4.23	119.1	0.00	0.0	1.76	0.00
150	90	2.40	-174.7	0.00	0.0	4.23	119.1	0.00	0.0	1.76	0.00
160	90	2.40	-174.7	0.00	0.0	4.23	119.1	0.00	0.0	1.76	0.00
170	90	2.40	-174.7	0.00	0.0	4.23	119.1	0.00	0.0	1.76	0.00
180	90	2.40	-174.7	0.00	0.0	4.23	119.1	0.00	0.0	1.76	0.00

TABLE 4.1d Stress in cm of water equivalent, strain in nanostrain, phase in deg. ($\lambda = \mu$ = 28 GPa)

O_1 Mean Stress		O_1 Dilatation		M_2 Mean Stress		M2 Dilatation		Ratio M_2/O_1 Stress
amp	phase	amp	phase	amp	phase	amp	phase	
3.21	5.4°	7.21	5.4°	5.61	-61.8°	12.58	-62.0°	1.75

TABLE 4.2 Mean stress (equivalent cm of water) and dilatation (nanostrain units) due to calculated body and load tides. ($\lambda = \mu$ = 28 GPa.)

	h_2	σ	ϕ_2	σ	h_1	σ	ϕ_1	σ	h2/h1
WELL W1									
Mean	5.04	0.41	-58.2	4.7	1.95	0.96	35.8	25.8	2.58
Median	4.93	0.17	-58.2	2.4	1.79	0.59	37.6	18.0	2.75
WELL W2									
Mean	4.90	0.14	-54.6	1.7	1.61	0.65	40.6	22.8	3.04
Median	4.83	0.14	-54.5	1.6	1.39	0.49	41.0	15.3	3.47

TABLE 5.1 Summary of 15 tidal analyses of well-level data for 1979-86. h_2 and h_1 are semidiurnal and diurnal constituents respectively in mm. ϕ_2 and ϕ_1 are phases of these constituents (deg) relative to the gravity tide.

AZ	VOLUMETRIC STRAIN (M2)		DIVIDED BY ISOTROPIC VOLUME STRAIN		VOLUMETRIC STRAIN (O1)		DIVIDED BY ISOTROPIC VOLUME STRAIN	
(deg)	amp	phase	amp	phase	amp	phase	amp	phase
0	4.06	-96.8	0.32	-34.8	2.80	15.7	0.39	10.3
10	5.48	-85.4	0.44	-23.4	2.99	25.1	0.41	19.7
20	7.09	-76.5	0.56	-14.5	3.29	30.5	0.46	25.1
30	8.71	-69.6	0.69	-7.6	3.60	32.1	0.50	26.7
40	10.14	-64.1	0.81	-2.1	3.86	30.5	0.54	25.1
50	11.17	-59.8	0.89	2.2	4.06	26.5	0.56	21.1
60	11.66	-56.1	0.93	5.9	4.22	20.7	0.59	15.3
70	11.55	-52.9	0.92	9.1	4.33	13.7	0.60	8.3
80	10.83	-50.0	0.86	12.0	4.42	6.2	0.61	0.8
90	9.57	-47.6	0.76	14.4	4.49	-1.1	0.62	-6.5
100	7.90	-45.5	0.63	16.5	4.51	-7.6	0.62	-13.0
110	6.02	-44.2	0.48	17.8	4.46	-12.9	0.62	-18.3
120	4.15	-45.0	0.33	17.0	4.31	-16.7	0.60	-22.1
130	2.51	-51.8	0.20	10.2	4.06	-18.5	0.56	-23.9
140	1.49	-76.4	0.12	-14.4	3.72	-17.8	0.52	-23.2
150	1.52	-110.7	0.12	-48.7	3.34	-14.1	0.46	-19.5
160	2.14	-117.8	0.17	-55.8	2.99	-6.8	0.41	-12.2
170	2.96	-109.3	0.24	-47.3	2.79	4.0	0.39	-1.4
180	4.06	-96.8	0.32	-34.8	2.80	15.7	0.39	10.3

TABLE 5.2 Volumetric strains (nanostrain) for the anistropic model formed from the isotropic case (Table 4.1) by forcing the strain in the azimuth=AZ+90 to be zero while leaving the strain in the azimuth=AZ the same. Phase in deg. (Poisson's ratio = .25)

DATE	TIME (UT)	MAG.	DIST. (KM)	AZ. (DEG)	Increase in Well Level (cm)
761023	20:58	4.2	52	54	-
770214	:35	3.1	7	262	-
770620	5:06	3.1	35	20	-
780526	2:32	3.2	32	55	-
790323	22:53	3.2	23	50	-
790819	22:49	5.1	35	70 *	-3.5
800701	3:06	3.8	33	267	-
800702	7:50	3.4	28	191	-
800702	7:57	3.2	28	191	-
800930	18:25	3.0	35	79	-
810315	19:43	3.0	18	353	-
810616	17:55	3.7	27	150	-
810706	20:48	3.1	8	193	-
820127	1:36	3.3	14	223	-
820829	2:07	3.4	20	201	-
821204	16:08	3.9	8	85 *	-5.4
830516	2:02	4.0	37	69	-
830602	6:30	3.4	14	137 *	-2.0
830604	4:58	3.0	37	172	-
841216	13:39	2.9	16	57	-
841222	12:46	3.0	17	161	-
850303	12:15	3.1	21	213	-
850410	05:53	3.1	28	96	-
860111	13:31	4.0	30	59 *	-3.7

TABLE 6.1 List of Charlevoix earthquakes of magnitude 3.0 or greater in the period 761023 to 860111. Residual water level changes are noted where clearly discernible.

Date & Mag'td	Observed Coseismic Strain (nanostrain)	Dist. (km)	Depth (km)	Radius of dil. zone R (km)	Required change in radius T (m)
830602	34.6	11	5.0	1	-6.28
	34.6	11	5.0	2	-1.57
Mag=3.4	34.6	11	5.0	3	-0.70
	34.6	11	5.0	4	-0.39
	34.6	11	5.0	5	
	34.6	11	5.0	6	
	34.6	11	5.0	7	
790819	60.5	35	10.2	1	-191.55
	60.5	35	10.2	2	-47.89
Mag=5.1	60.5	35	10.2	3	-21.28
	60.5	35	10.2	4	-11.97
	60.5	35	10.2	5	-7.66
	60.5	35	10.2	6	-5.32
	60.5	35	10.2	7	-3.91
	60.5	35	10.2	8	-2.99
	60.5	35	10.2	9	-2.36
	60.5	35	10.2	10	-1.92
821204	93.1	8	15.3	1	17.67
	93.1	8	15.3	2	4.42
Mag=3.9	93.1	8	15.3	3	1.96
	93.1	8	15.3	4	1.10
	93.1	8	15.3	5	0.71
	93.1	8	15.3	6	0.49
	93.1	8	15.3	7	0.36
	93.1	8	15.3	8	0.28
	93.1	8	15.3	9	0.22
	93.1	8	15.3	10	0.18
860111	63.9	30	4.7	1	-96.39
	63.9	30	4.7	2	-24.10
Mag=4.0	63.9	30	4.7	3	-10.71
	63.9	30	4.7	4	-6.02
	63.9	30	4.7	5	
	63.9	30	4.7	6	
	63.9	30	4.7	7	

TABLE 6.2. The loss of dilatancy of a spherical dilatant zone of given radius required to account for the observed volume strain at the well after four earthquakes. Loss of dilatancy is assumed coincident with draining of the suddenly pressurized dilatant zone to the surrounding region and is represented here as 1% of the volume of the outer shell of thickness T (ie. 1% porosity). The entire zone will eventually drain, at a decreasing rate, but it is assumed here that the observed strain is due entirely to draining of this outer most part of the sphere. A negative sign denotes a loss of dilatancy. The model requires an increase in dilatancy after the earthquake of 821204. (Calculation based on Hagiwara, 1977).

FIGURE CAPTIONS

Figure 1.1 The Charlevoix Geodynamics Observatory near Charlevoix, Quebec. Showing the observation wells (OBS): W1, W2, W3 and the cased boreholes: BT1, BT2 and BT3. Uncased sections indicated by dashed lines.

Figure 2.1 Comparison of Observed (dashed) and Predicted Well Levels for the Year 1979.

Figure 2.2 Comparison of Observed (dashed) and Predicted Well Levels for the Year 1980.

Figure 2.3 Comparison of Observed (dashed) and Predicted Well Levels for the Year 1981.

Figure 2.4 Comparison of Observed (dashed) and Predicted Well Levels for the Year 1982.

Figure 2.5 Comparison of Observed (dashed) and Predicted Well Levels for the Year 1983.

Figure 2.6 Comparison of Observed (dashed) and Predicted Well Levels for the Year 1984.

Figure 2.7 Comparison of Observed (dashed) and Predicted Well Levels for the Year 1985

Figure 3.1 Illustrating the Determination of Barometric Efficiency, 26%, 1979.

Figure 3.2 Illustrating the Determination of Barometric Efficiency, 24%, 1982.

Figure 3.3 Illustrating the Determination of Barometric Efficiency, 13%, 1985.

Figure 3.4 Illustrating the Determination of Barometric Efficiency, 22%, 1986.

Figure 5.1 Ratio of predicted semidurnal (h_2) and diurnal (h_1) linear strains in given direction. Also shown are ratio of predicted volumetric strain amplitudes (volumetric ratio) and ratio of observed welll-tide amplitudes (observed ratio).

Figure 5.2 Predicted phase of O_1 linear strain in given direction. Also shown is observed well-tide phase (observed phase) and predicted phase of volumetric strain (volumetric phase).

Figure 5.3 Predicted phase of M_2 linear strain in given direction. Also shown are predicted phase of M2 volumetric strain (volumetric phase) and phase of observed M_2 well tide (observed phase).

Figure 5.4 Showing the variation with time of the M_2 well level tide (amplitude and phase), 1981-1985.

Figure 5.5 Amplitude (in equivalent cm. of water) and phase (in deg.) of the horizontal tidal stress (total body and load M_2 constituent) components in the azimuths AZ and AZ-90°. The sum of these two components (divided by 3) is the mean normal stress: 5.6 cm and -61.9°. The ratio column lists the ratio of the stress in the azimuth AZ to the mean normal stress and is intended as a prediction of the ratio of the well-level tide for the anistropic case (zero stress in the azimuth AZ-90°) to the well-level for the isotropic case.

Figure 6.1 Comparison of observed well level, corrected for tides, barometric effect and an exponential decay, with the predicted water level. A magnitude 5.1 earthquake occurred on day 231 att 22:19.

Figure 6.2 Detail from Figure 6.1.

Figure 6.3 Comparison of unedited well level (solid line) with a fitted exponential decay. Note the earthquake on day 231 (Magnitude 5.1 at 22:49)

Figure 6.4 Well level detail near the 1982 earthquake (Magnitude 3.9, day 338 at 16:08).

Figure 6.5 Comparison of observed well level, corrected for tides and barometric effect, with the predicted water level near the time of the 1982 earthquake (Magnitude 3.9, day 338 at 16:08)

Figure 6.6 Comparison of observed well level, corrected for tides but not barometric effect, with the predicted water level near the time of the 1983 earthquake (day 153 at 06:30).

Figure 6.7 Well level detail near the 1983 earthquake (day 153 at 06:30)

Figure 6.8 Comparison of corrected observed well level (solid line) with uncorrected water level about the time of the 1986 earthquake (day 11 at 03:31, magnitude 4.0).

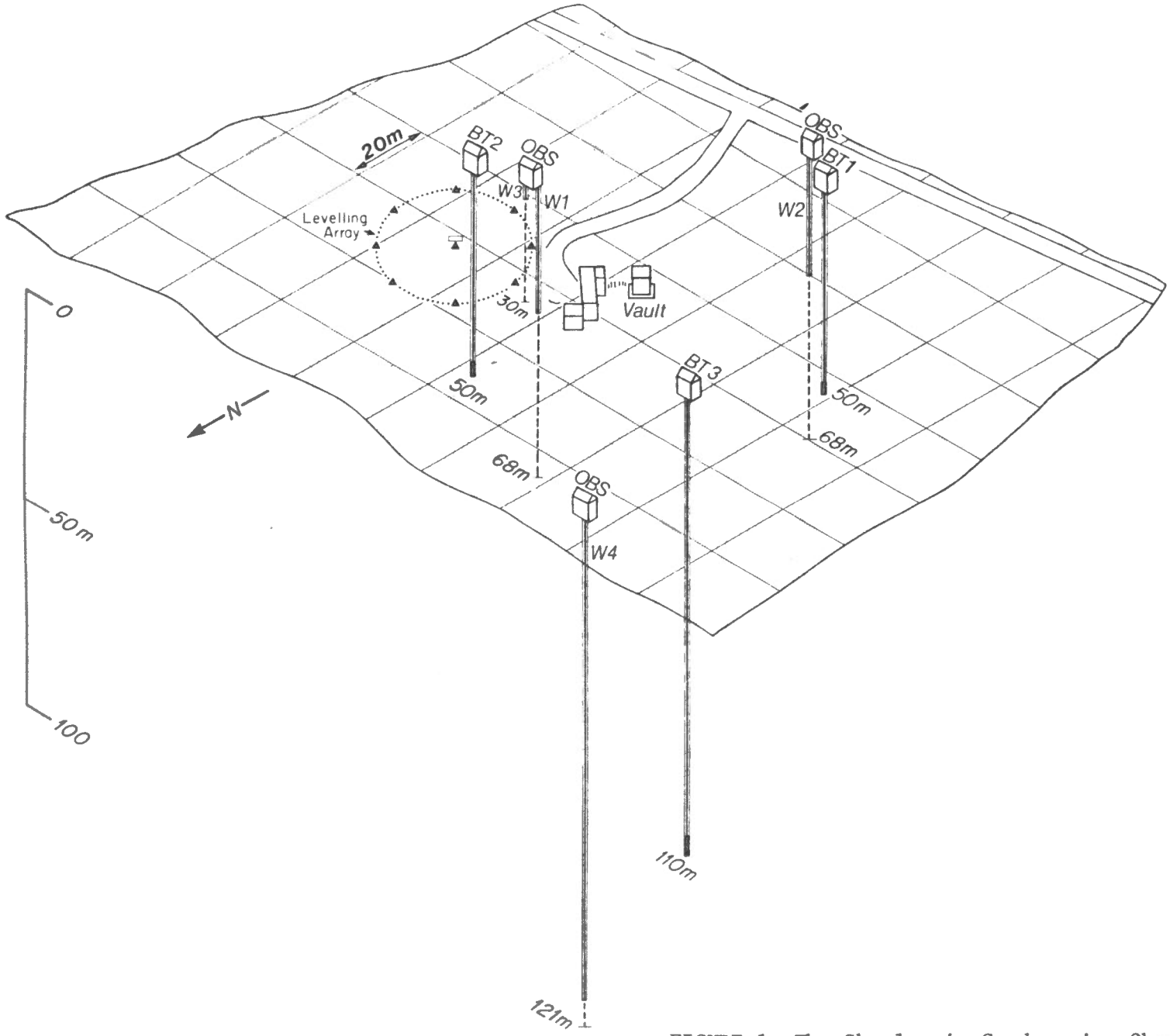

FIGURE 1. The Charlevoix Geodynamics Observatory

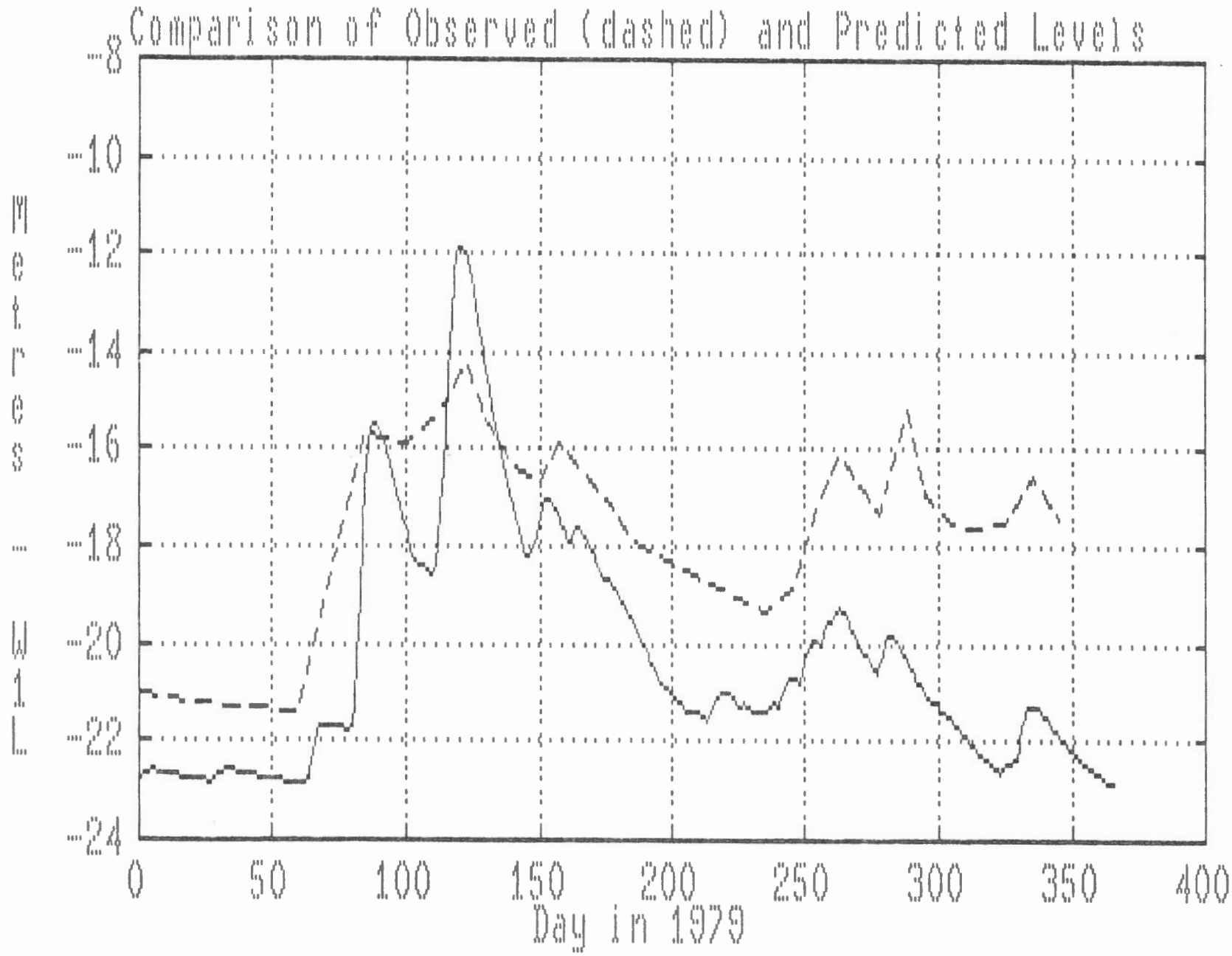
Comparison of Observed (dashed) and Predicted Levels
Meters - WL
-8
-10
-12
-14
-16
-18
-20
-22
-24
0
50
100
150
200
250
300
350
400
Day in 1979

FIGURE 2.1

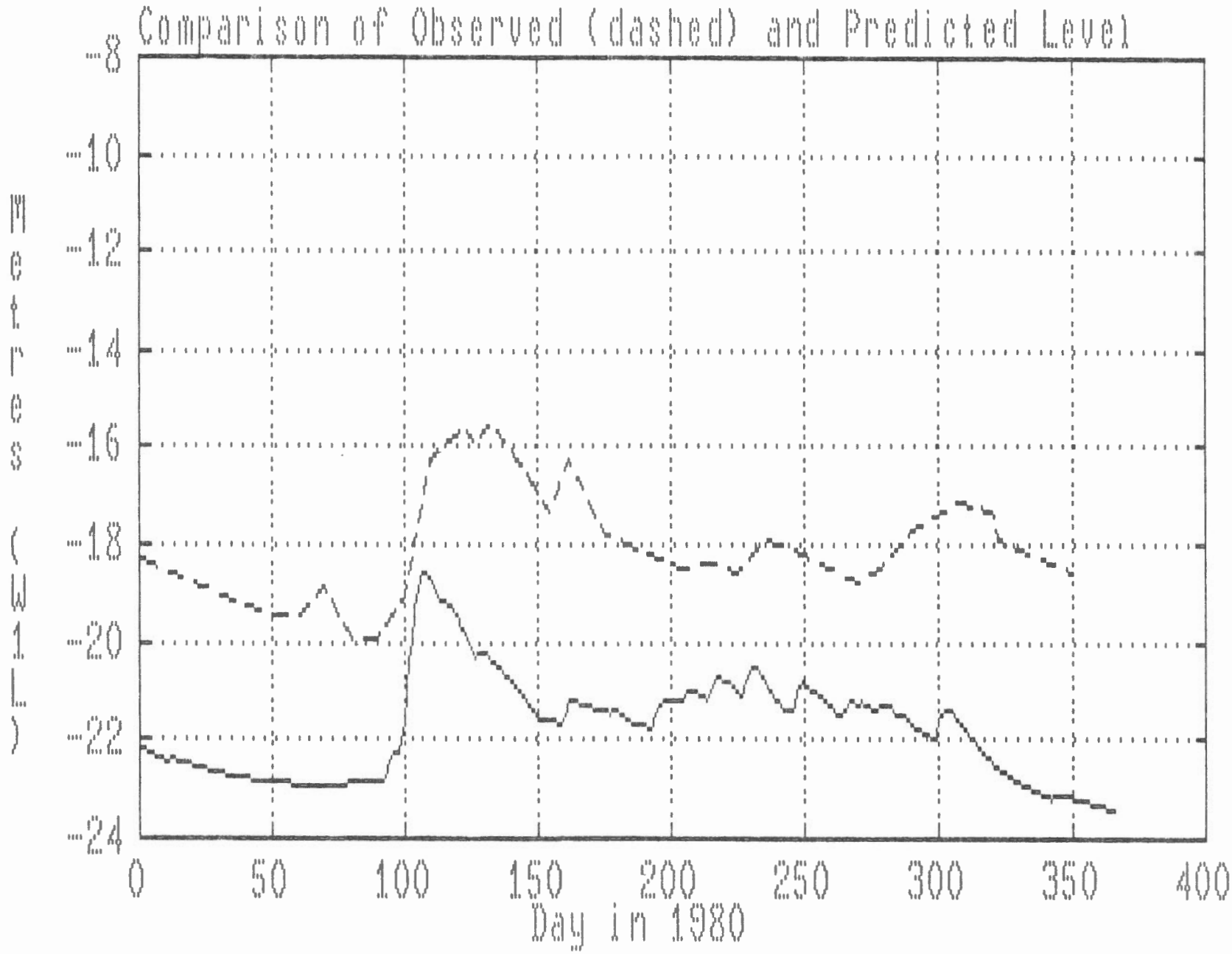
Comparison of Observed (dashed) and Predicted Level
Meters (MSL)
-8
-10
-12
-14
-16
-18
-20
-22
-24
0
50
100
150
200
250
300
350
400
Day in 1980

FIGURE 2.2

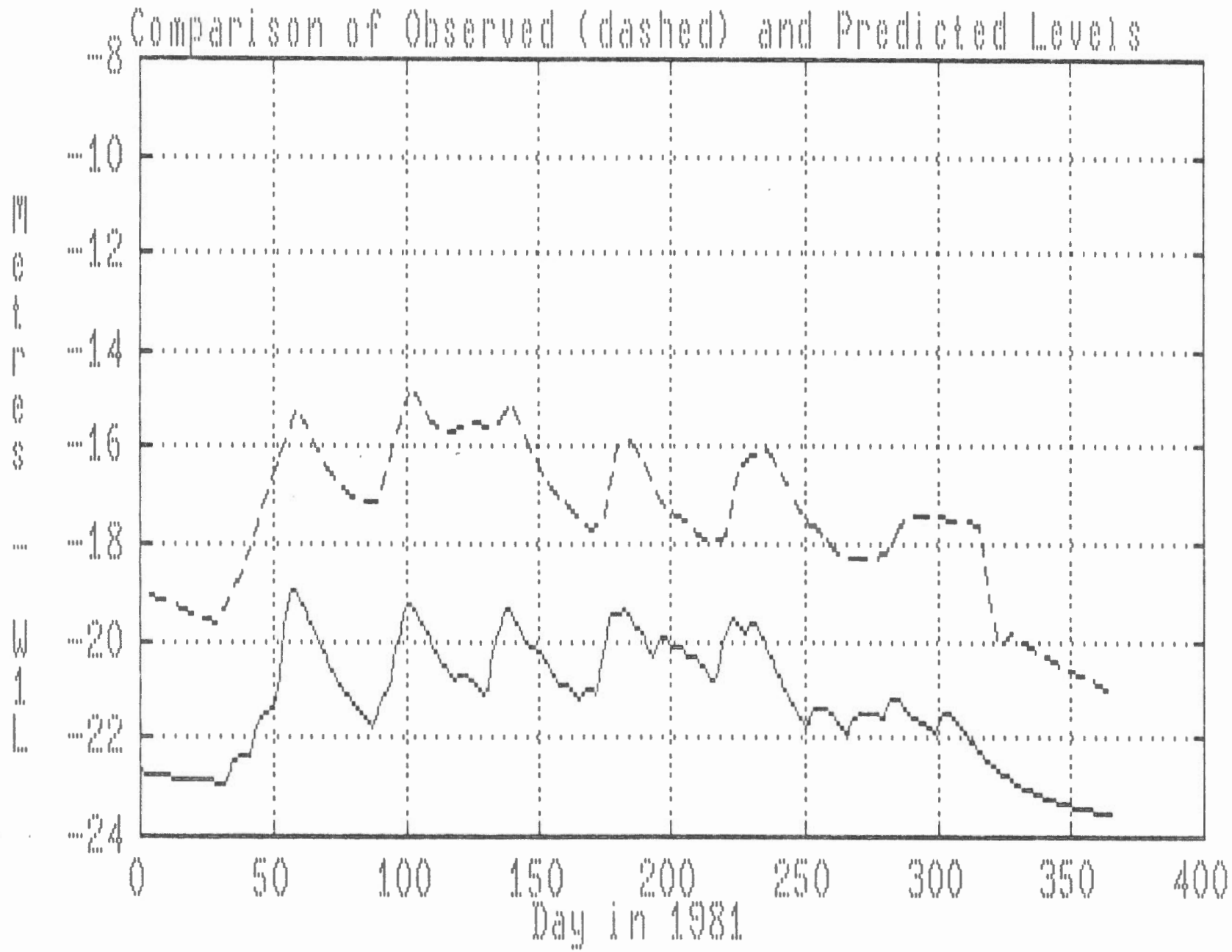
Comparison of Observed (dashed) and Predicted Levels
Meters - WL
-8
-10
-12
-14
-16
-18
-20
-22
-24
0
50
100
150
200
250
300
350
400
Day in 1981

FIGURE 2.3

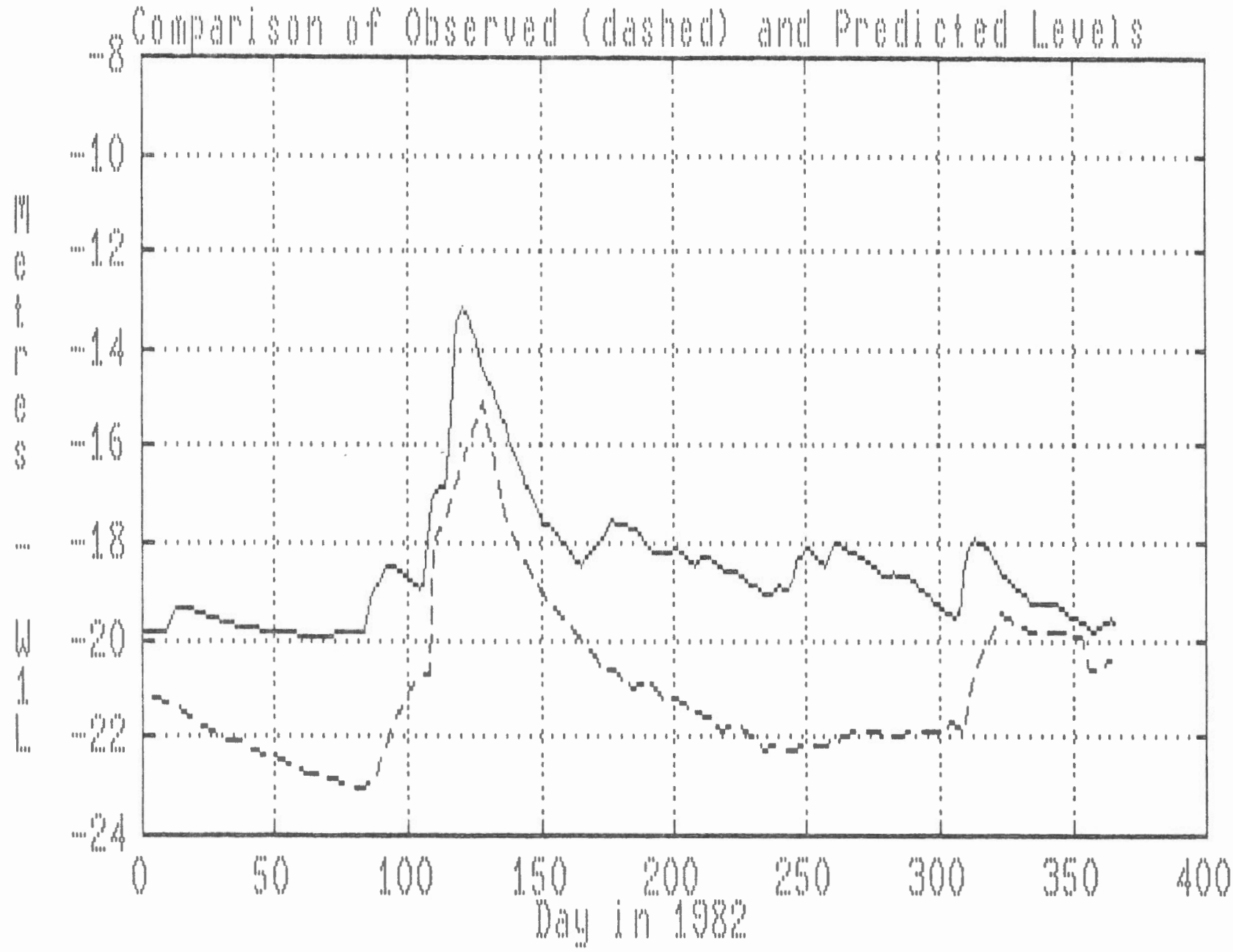
Comparison of Observed (dashed) and Predicted Levels
Meters - MSL
-8
-10
-12
-14
-16
-18
-20
-22
-24
0
50
100
150
200
250
300
350
400
Day in 1982

FIGURE 2.4

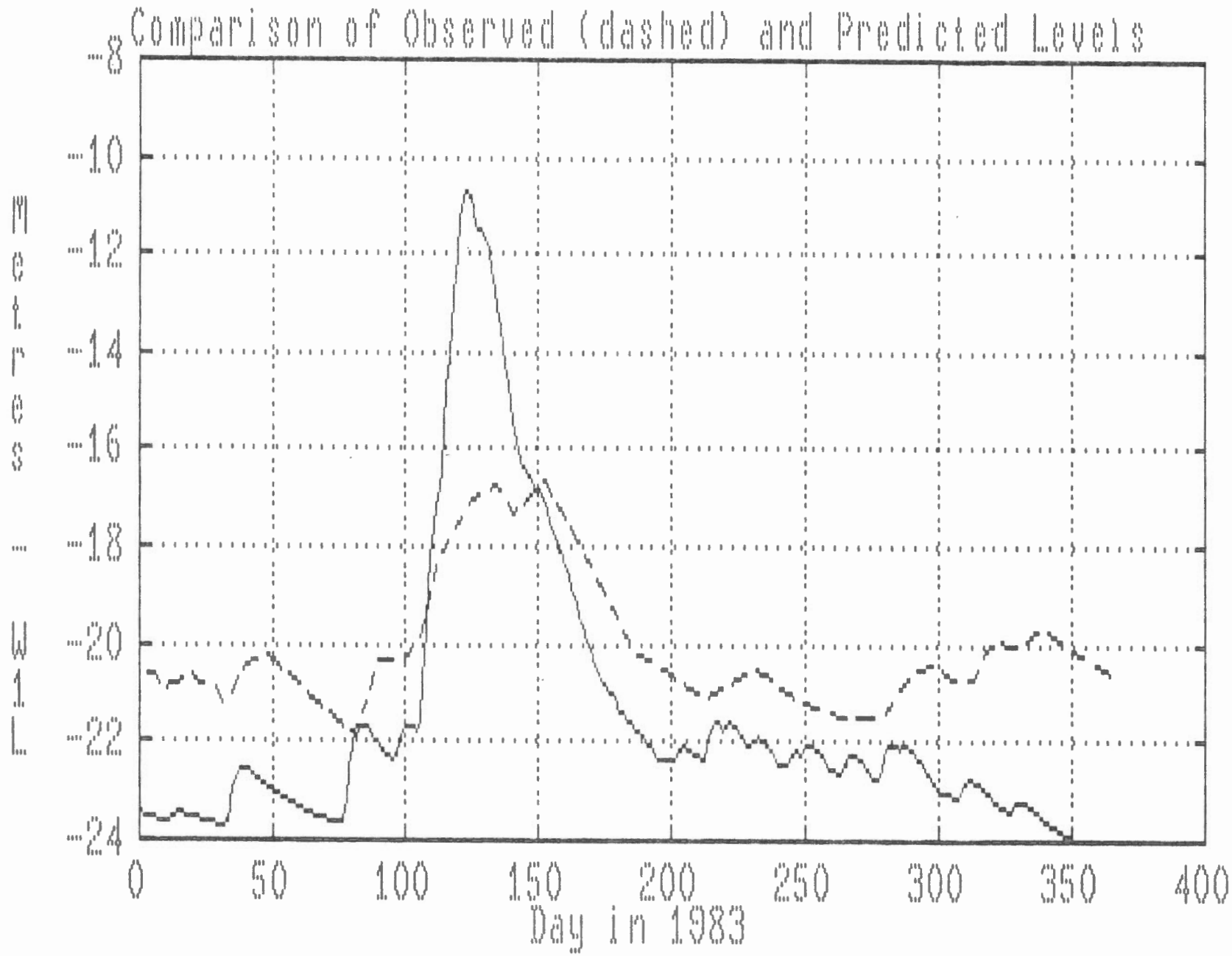
Comparison of Observed (dashed) and Predicted Levels
Meters - MWL
-8
-10
-12
-14
-16
-18
-20
-22
-24
0
50
100
150
200
250
300
350
400
Day in 1983

FIGURE 2.5

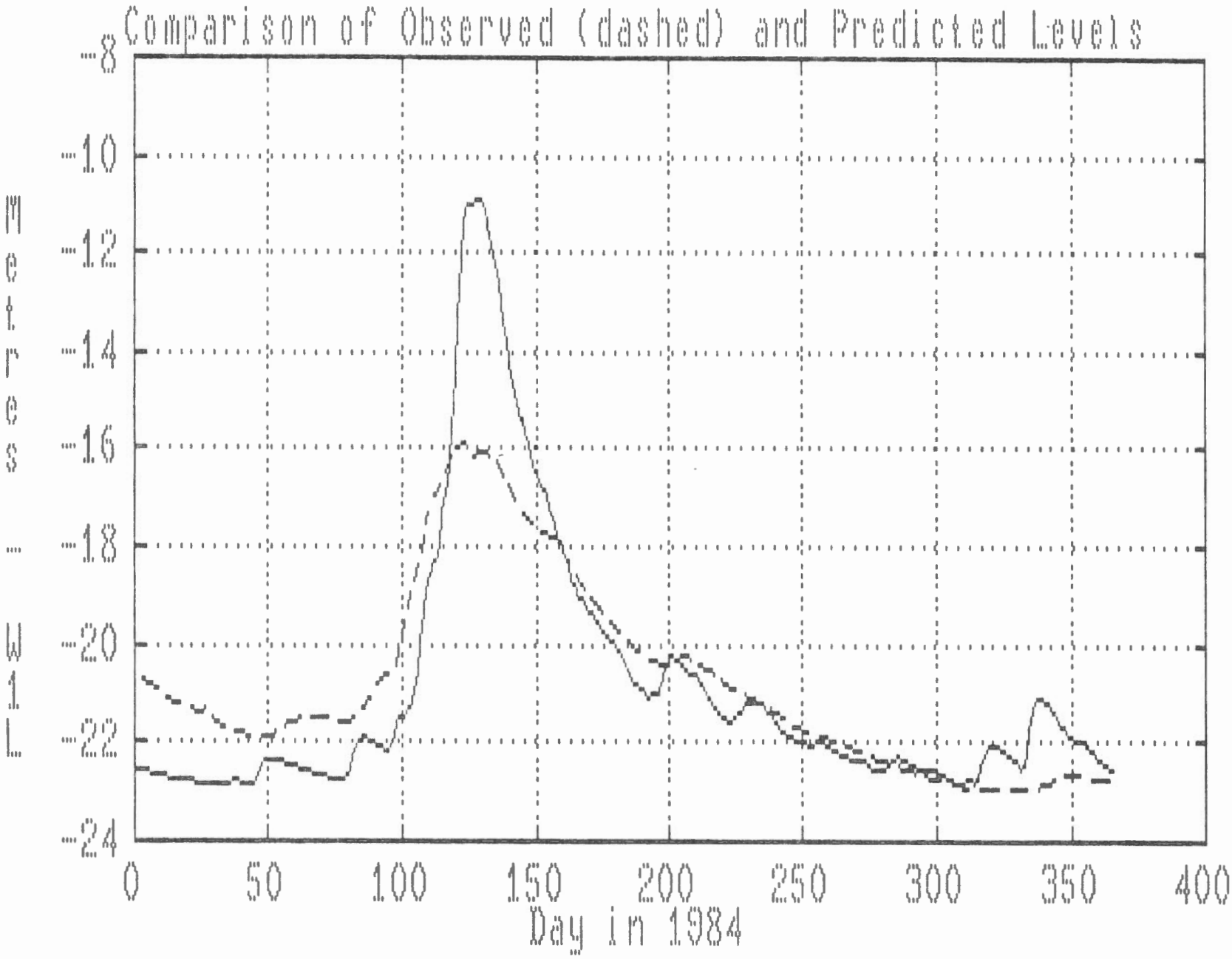
Comparison of Observed (dashed) and Predicted Levels
Level - meters
-8
-10
-12
-14
-16
-18
-20
-22
-24
0
50
100
150
200
250
300
350
400
Day in 1984

FIGURE 2.6

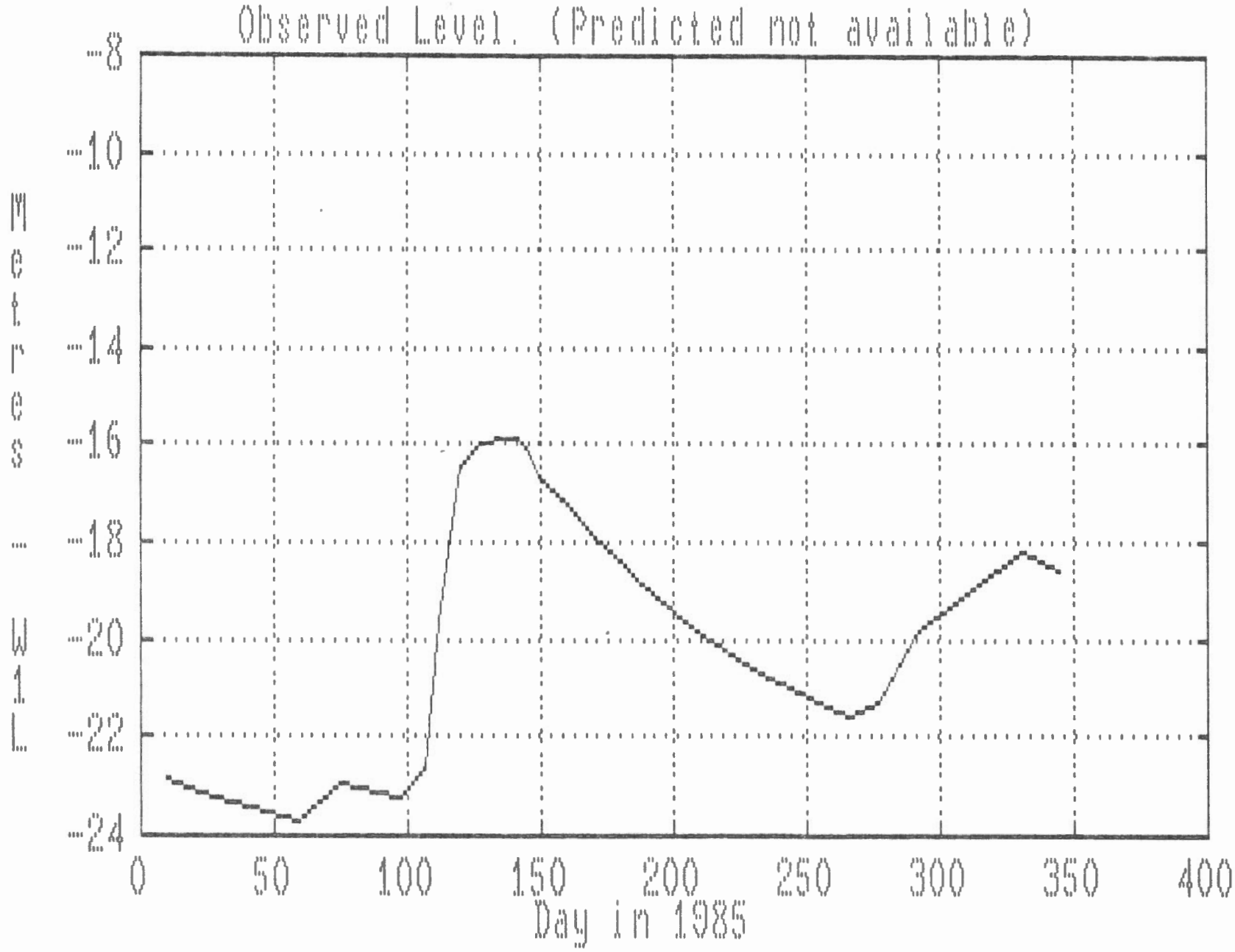
Observed Level. (Predicted not available)
Metres - WLL
-8
-10
-12
-14
-16
-18
-20
-22
-24
0
50
100
150
200
250
300
350
400
Day in 1985

FIGURE 2.7

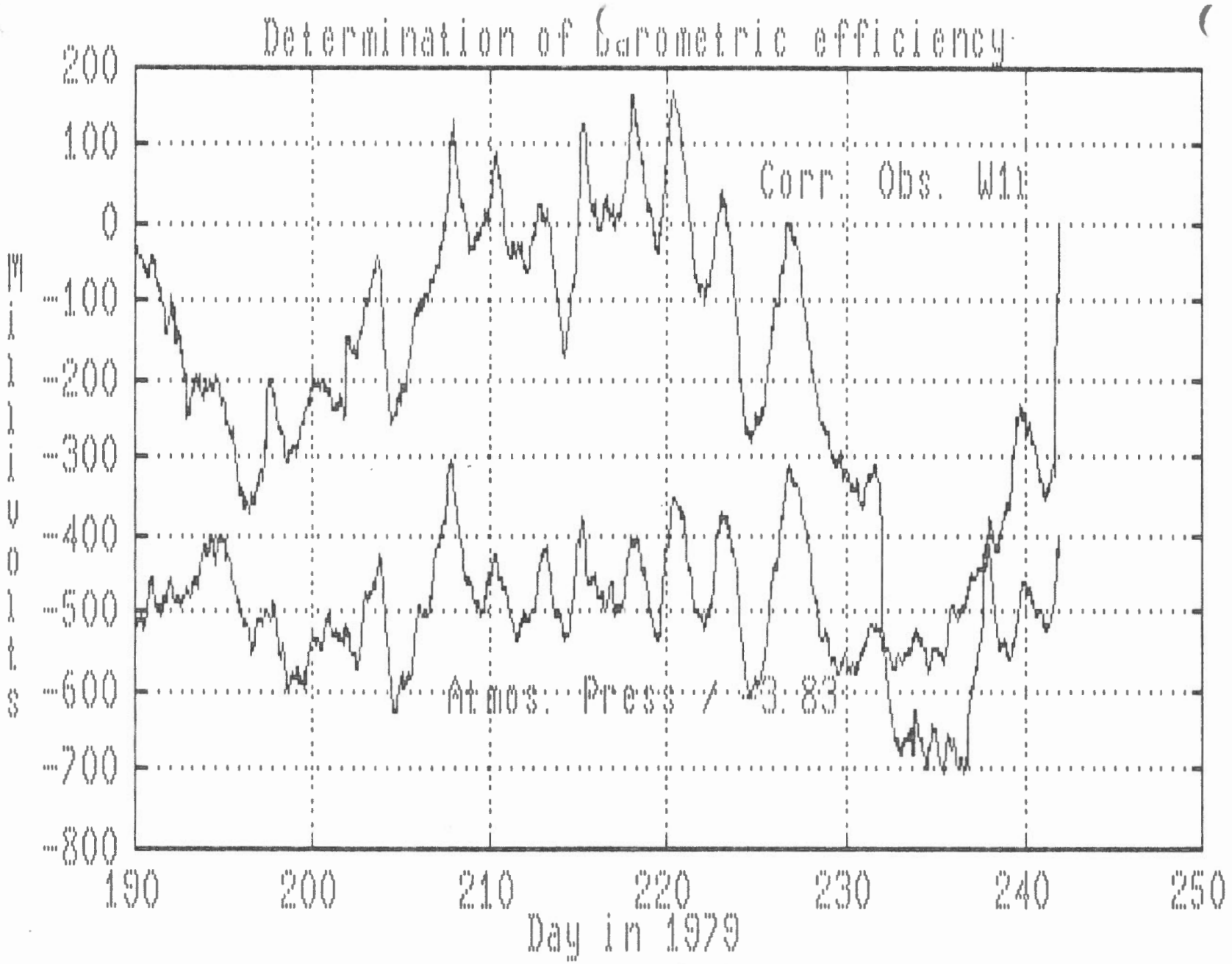
Determination of barometric efficiency
Corr. Obs. W1
Atmos. Press / 3.83
Millivolts
200
100
0
-100
-200
-300
-400
-500
-600
-700
-800
190
200
210
220
230
240
250
Day in 1979

FIGURE 3.1

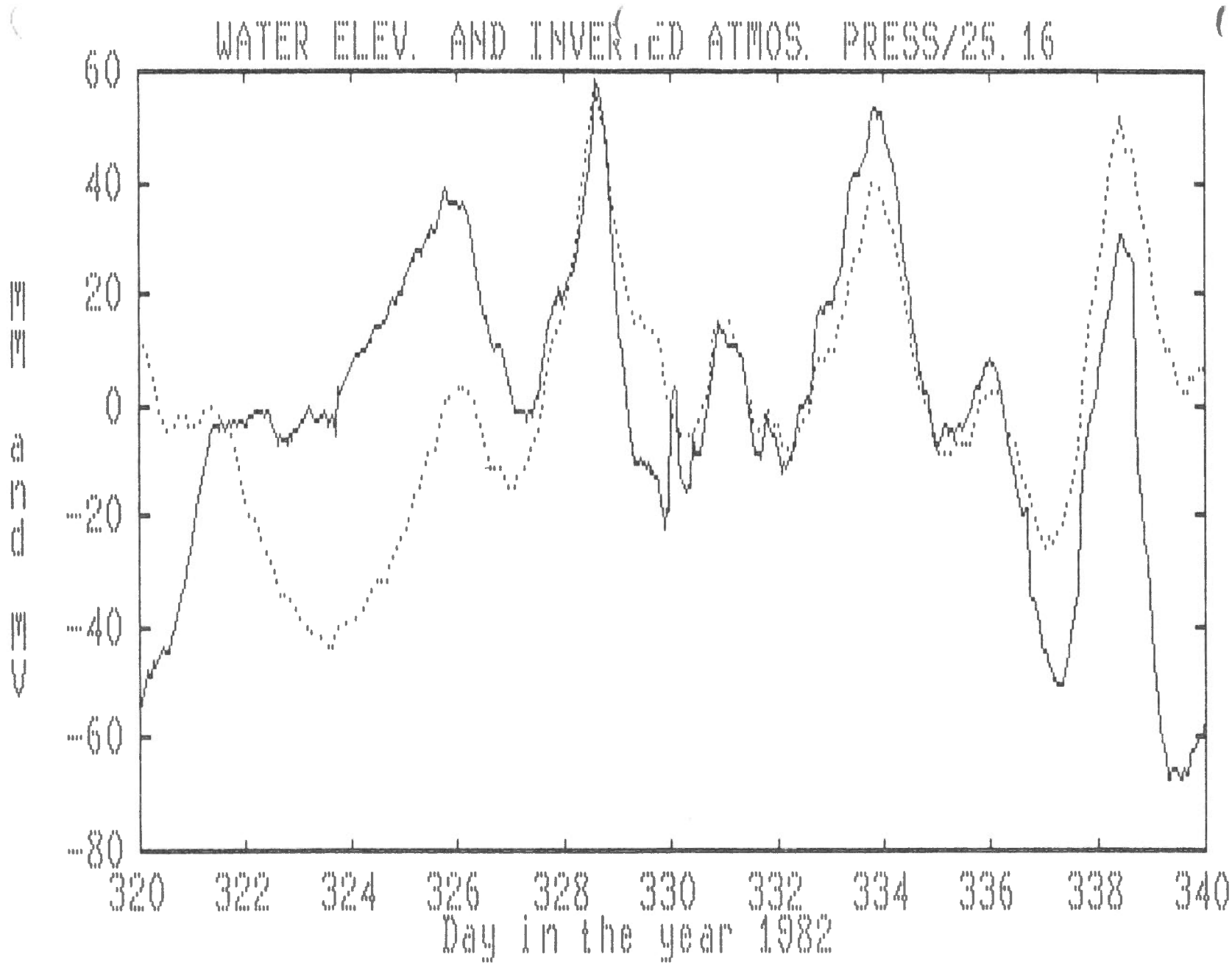
WATER ELEV. AND INVER.ED ATMOS. PRESS/25.16
60
40
20
0
-20
-40
-60
-80
320
322
324
326
328
330
332
334
336
338
340
Day in the year 1982

FIGURE 3.2

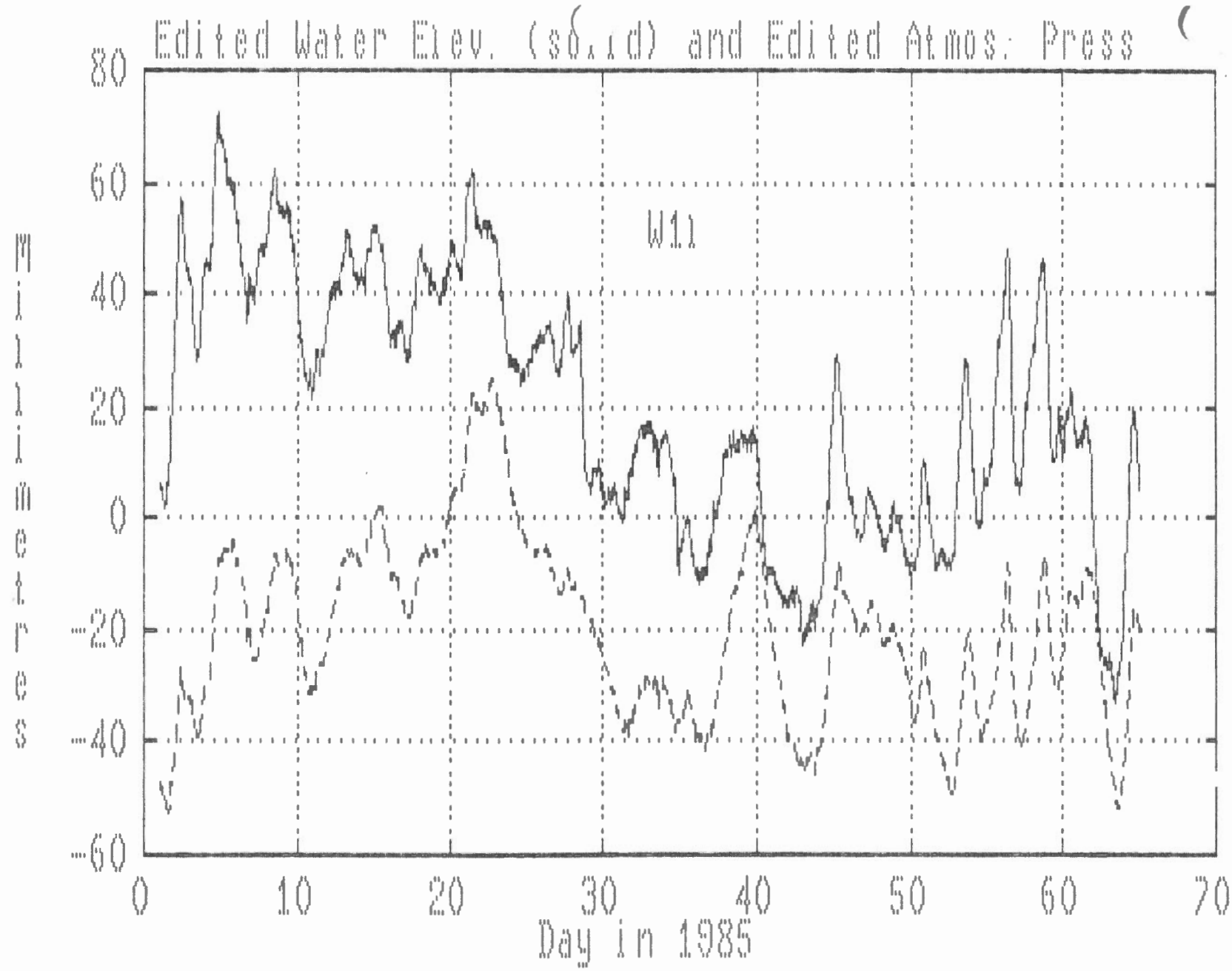
Edited Water Elev. (s6.1d) and Edited Atmos. Press
W11
Millimetres
80
60
40
20
0
-20
-40
-60
0
10
20
30
40
50
60
70
Day in 1985

FIGURE 3.3

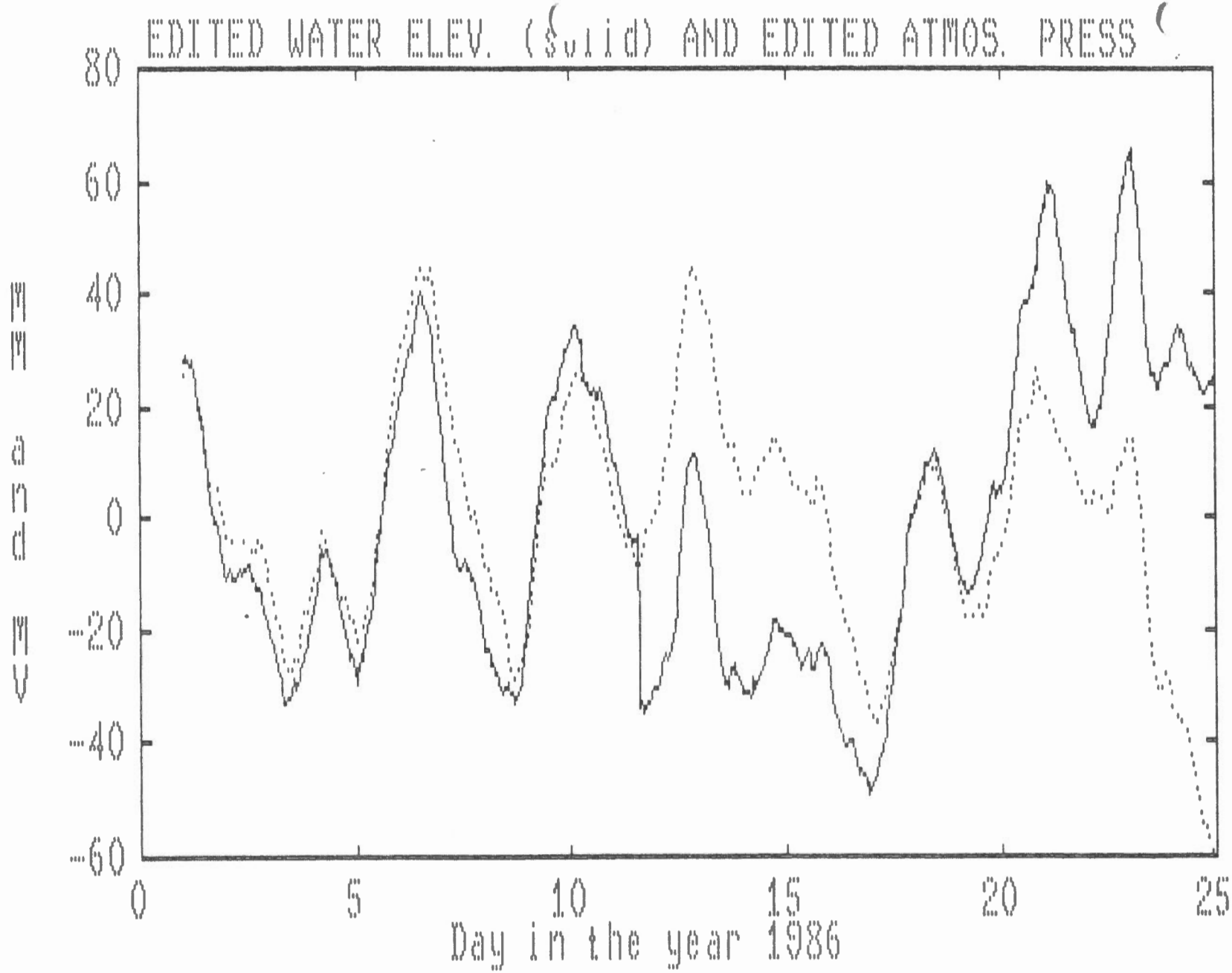
EDITED WATER ELEV. (Solid) AND EDITED ATMOS. PRESS
80
60
40
20
0
-20
-40
-60
MB and MV
0
5
10
15
20
25
Day in the year 1986

FIGURE 3.4

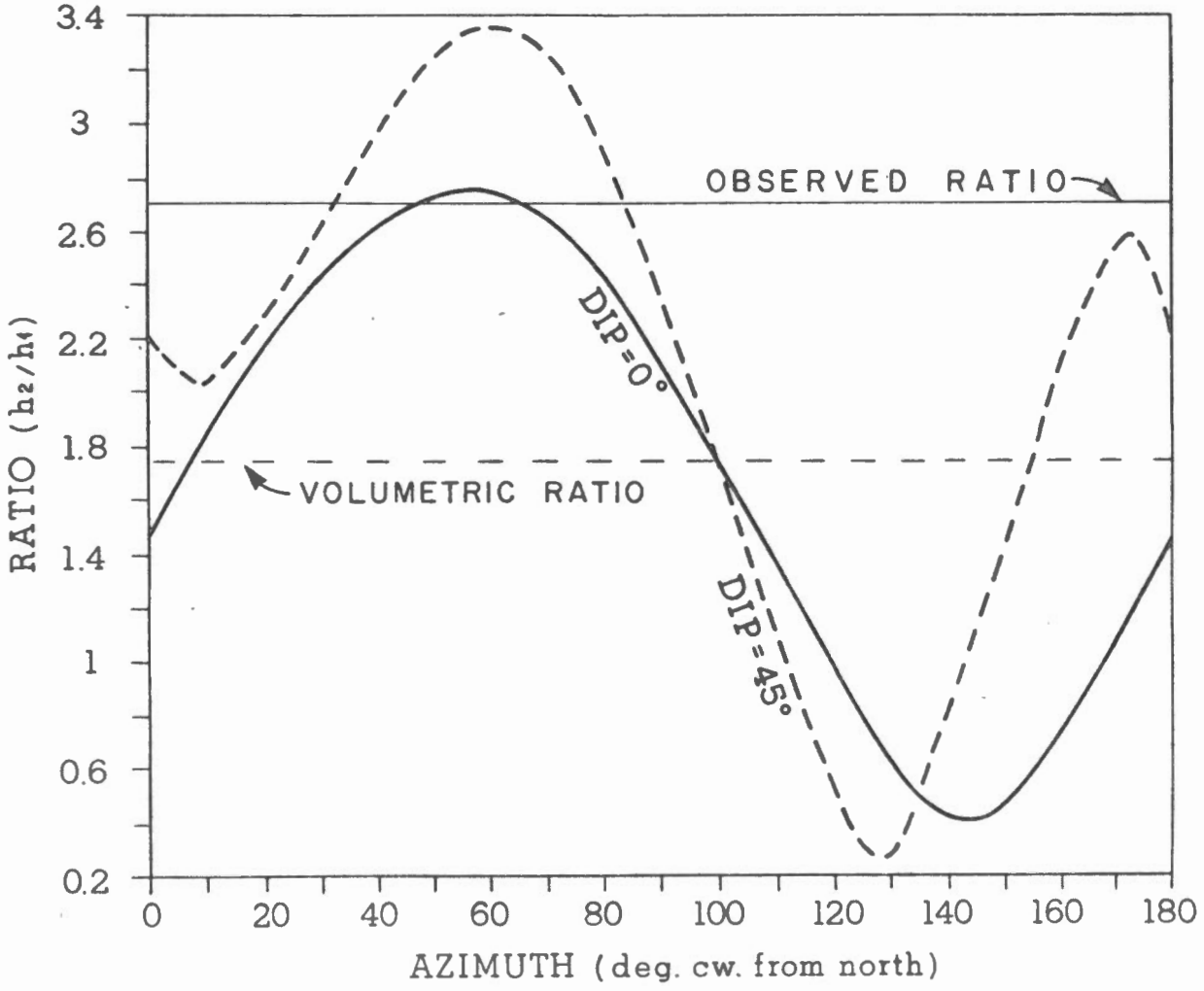
3.4
3
2.6
2.2
1.8
1.4
1
0.6
0.2
RATIO (h2/h1)
OBSERVED RATIO
DIP=0°
VOLUMETRIC RATIO
DIP=45°
0
20
40
60
80
100
120
140
160
180
AZIMUTH (deg. cw. from north)

FIGURE 5.1

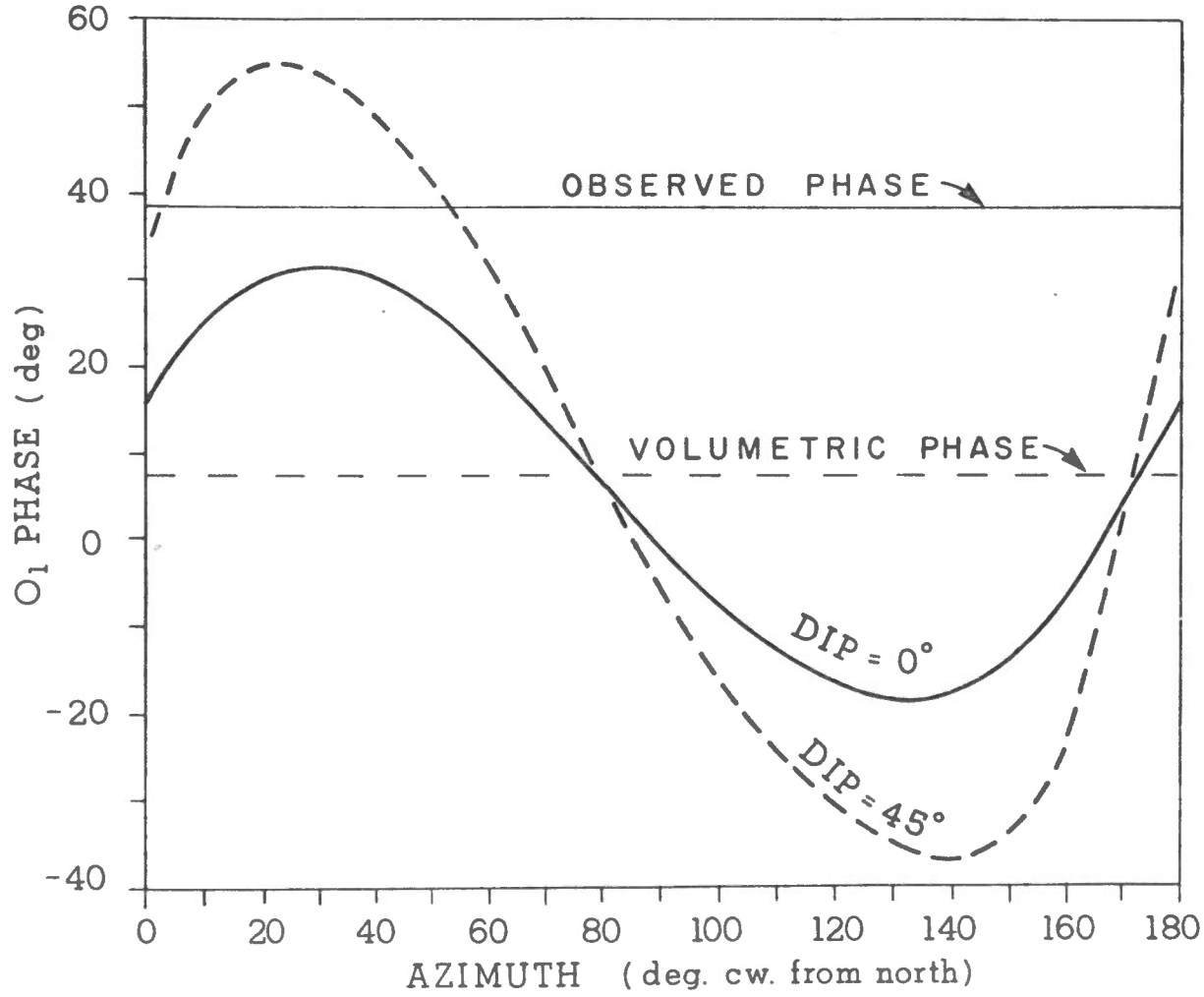
60
40
20
0
-20
-40
O_1 PHASE (deg)
OBSERVED PHASE
VOLUMETRIC PHASE
DIP = 0°
DIP = 45°
0
20
40
60
80
100
120
140
160
180
AZIMUTH (deg. cw. from north)

FIGURE 5.2

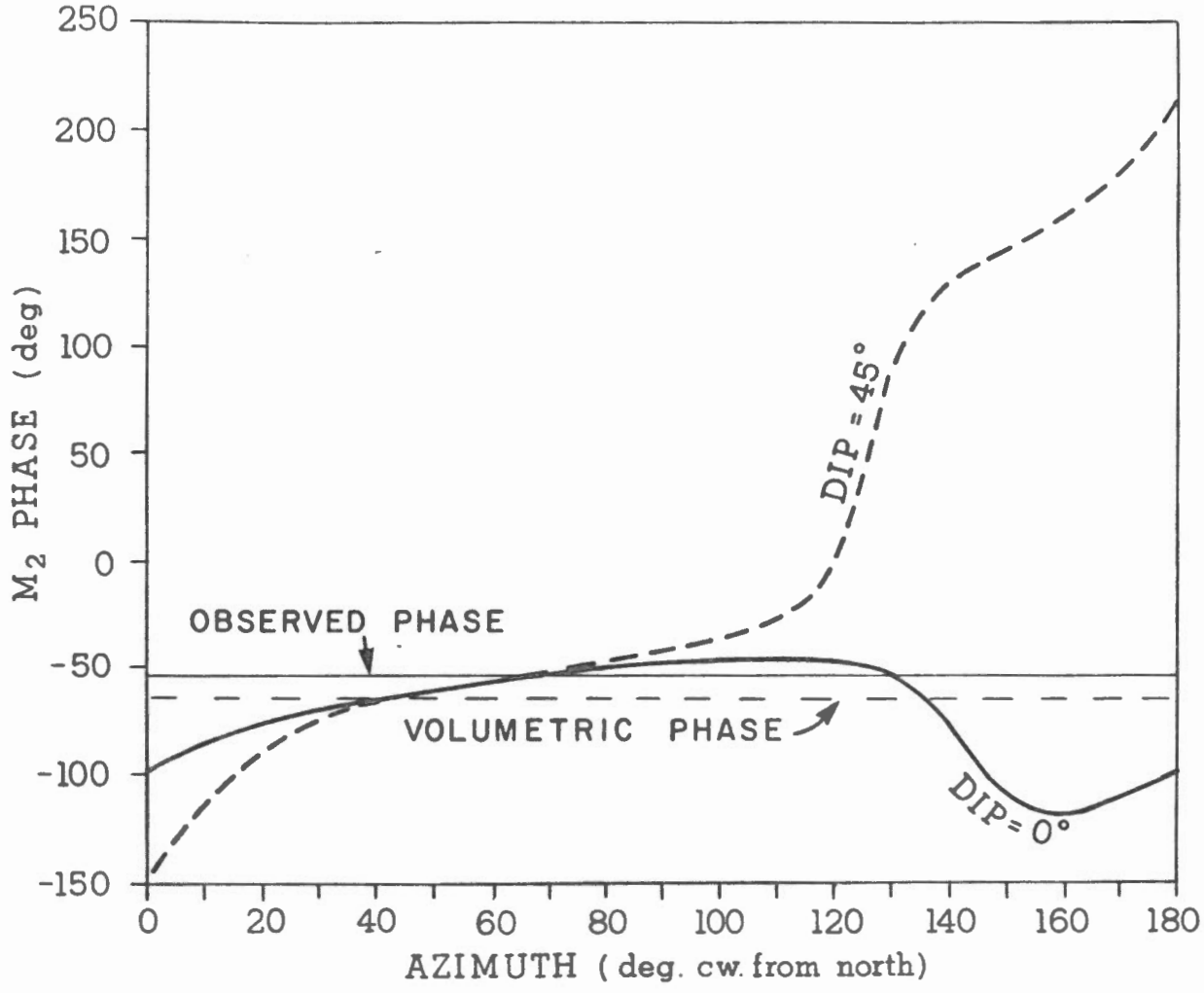
250
200
150
100
50
0
-50
-100
-150
M_2 PHASE (deg)
OBSERVED PHASE
VOLUMETRIC PHASE
DIP = 45°
DIP = 0°
0
20
40
60
80
100
120
140
160
180
AZIMUTH (deg. cw. from north)

FIGURE 5.3

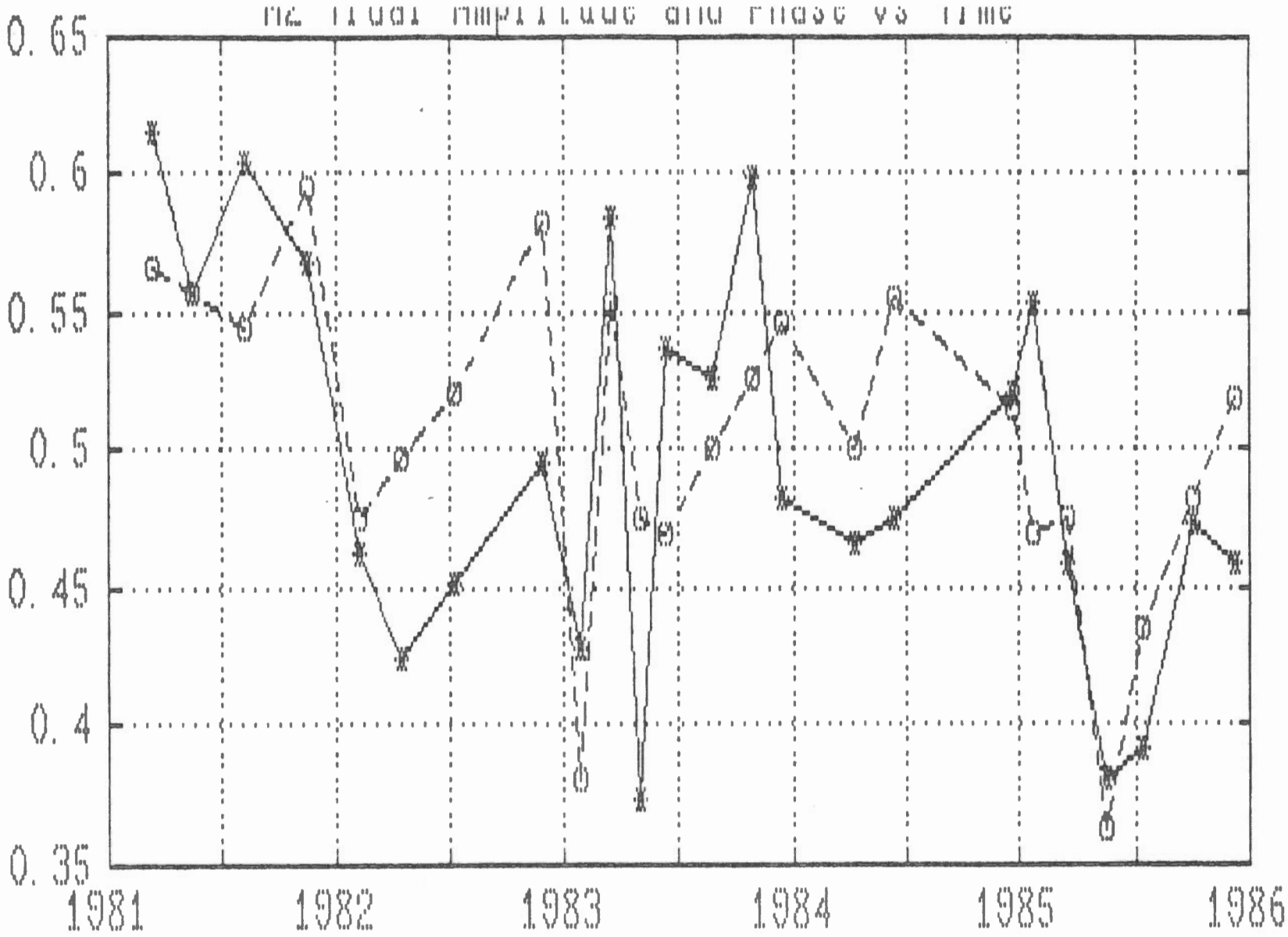

FIGURE 5.4

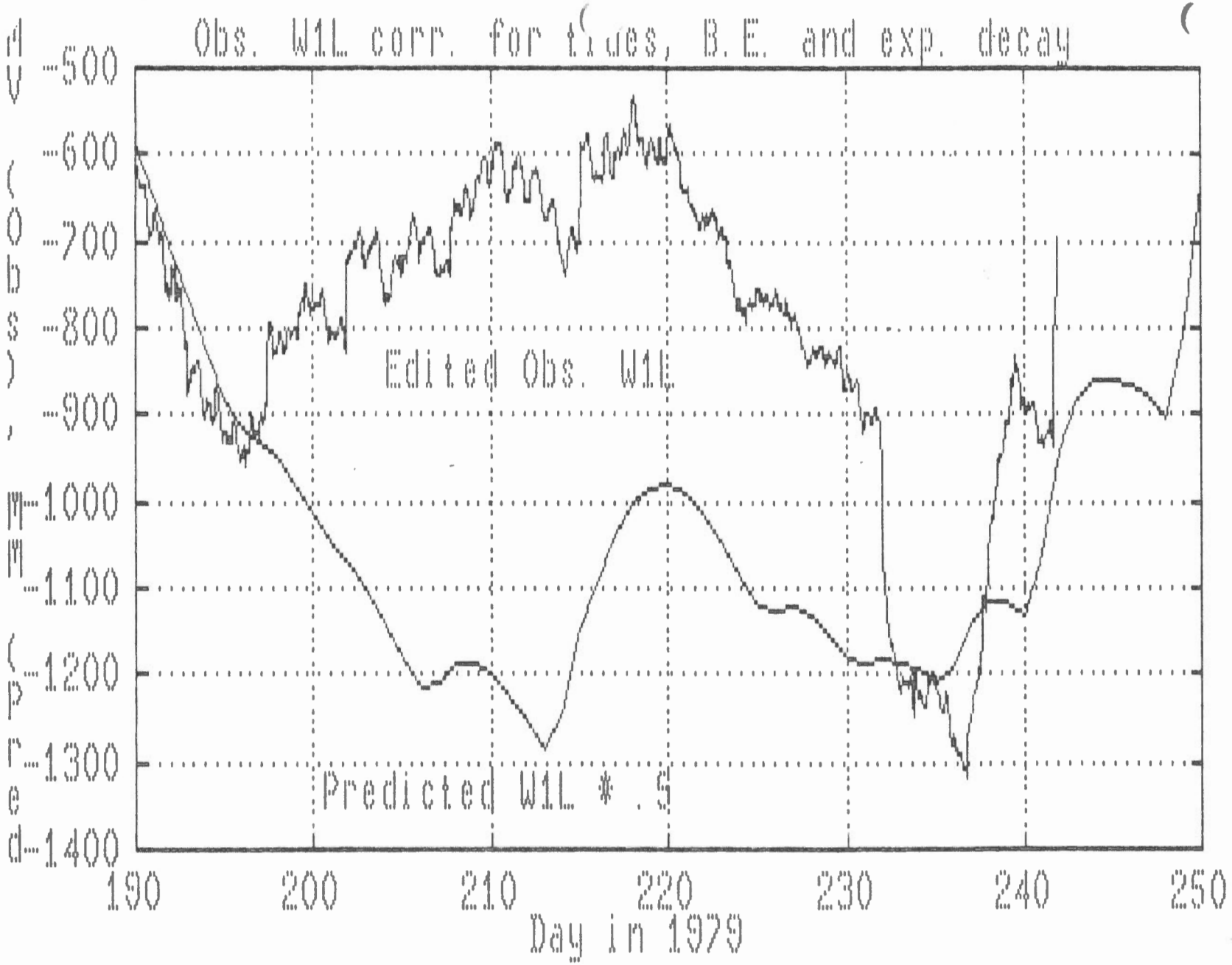
Obs. WtL corr. for tides, B.E. and exp. decay
Edited Obs. WtL
Predicted WtL * .5
-500
-600
-700
-800
-900
-1000
-1100
-1200
-1300
-1400
190
200
210
220
230
240
250
Day in 1979

FIGURE 6.1


Obs. WIL corr. for f.des, B.E. and exp. decay
-800
-900
-1000
-1100
-1200
-1300
-1400
Millivolts
230
231
232
233
234
235
236
237
238
239
240
Day in 1979

FIGURE 6.2

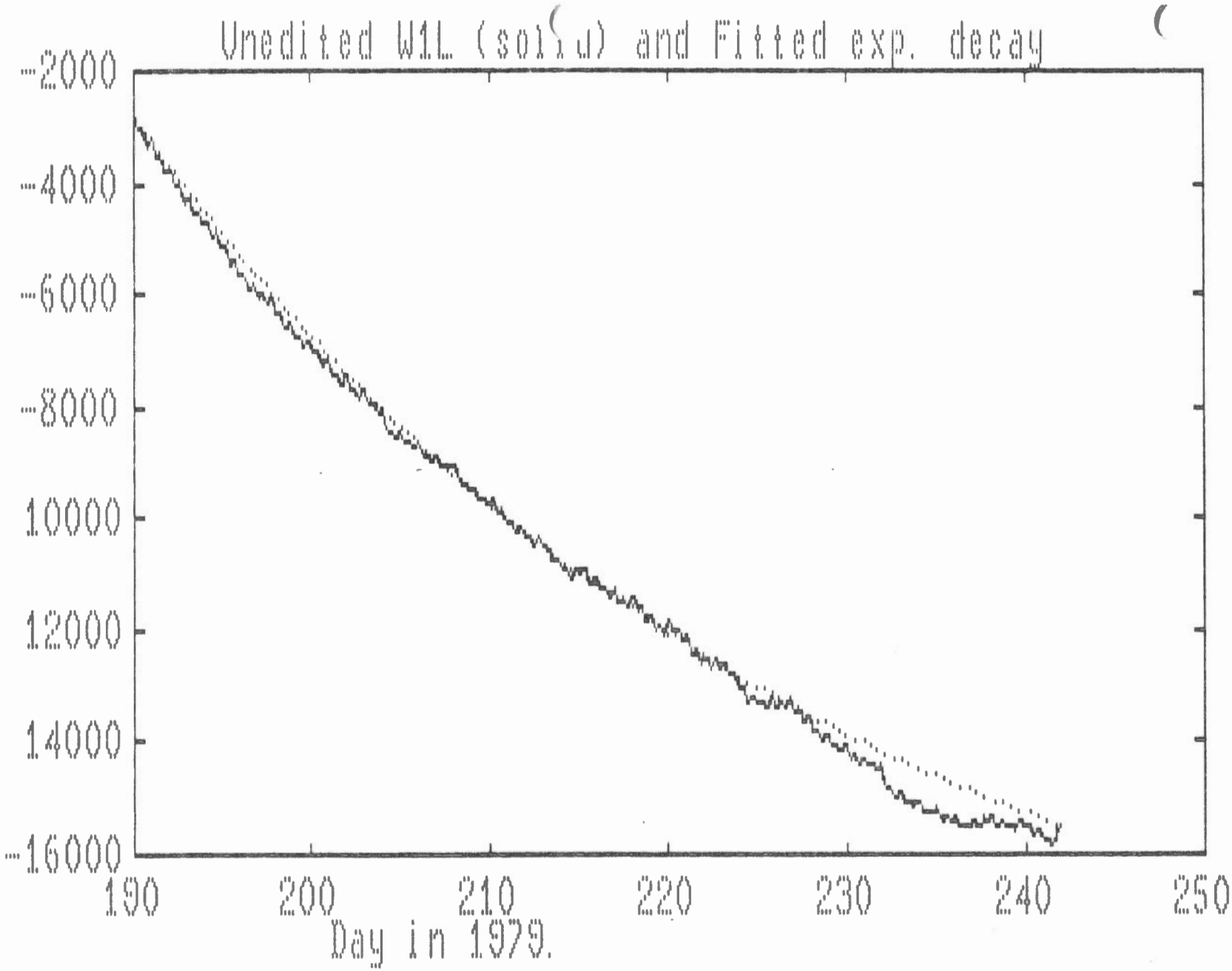
Unedited WIL (soil) and Fitted exp. decay
-2000
-4000
-6000
-8000
10000
12000
14000
-16000
190
200
210
220
230
240
250
Day in 1979.

FIGURE 6.3

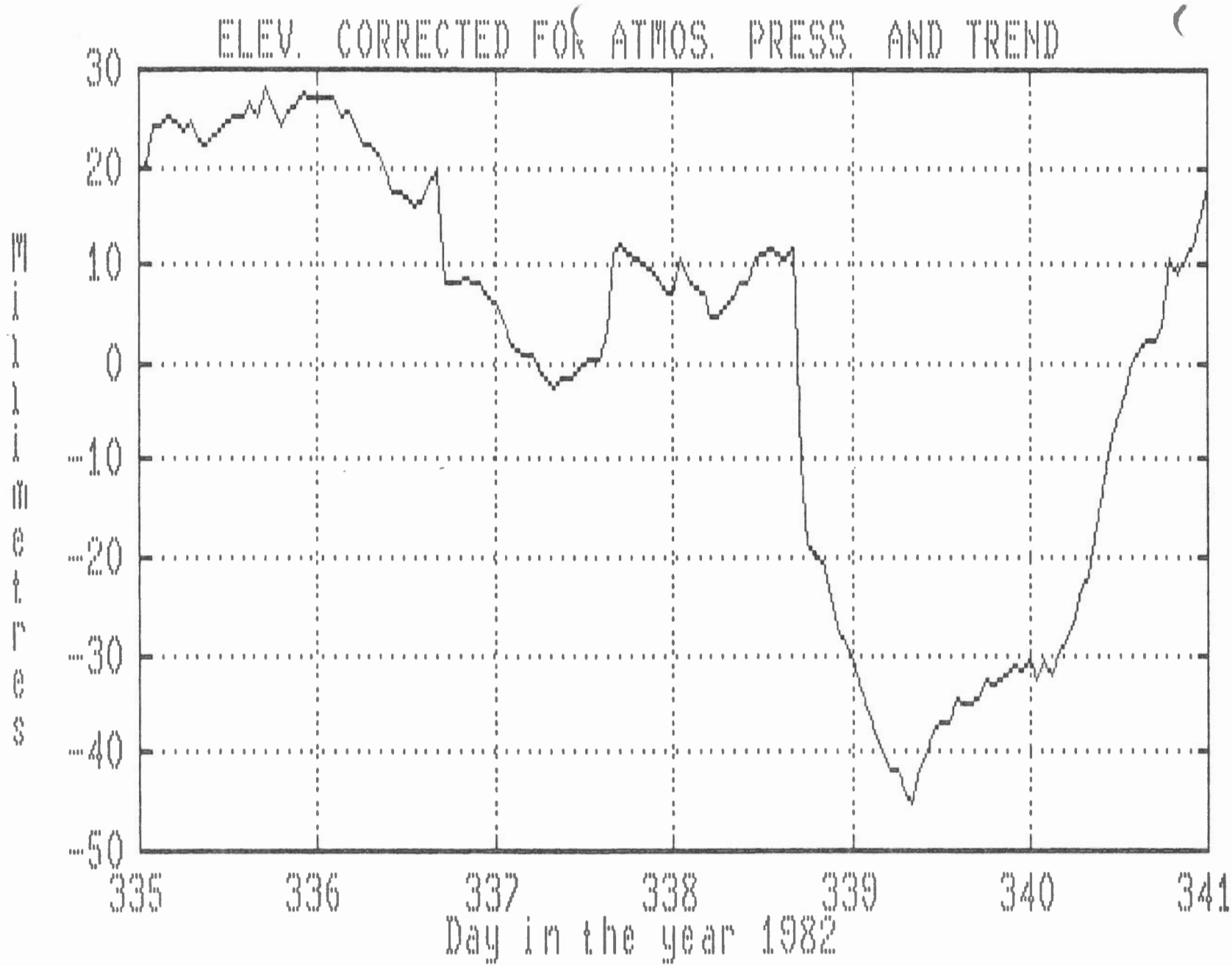
ELEV. CORRECTED FOR ATMOS. PRESS. AND TREND
30
20
10
0
-10
-20
-30
-40
-50
Meters
335
336
337
338
339
340
341
Day in the year 1982

FIGURE 6.4

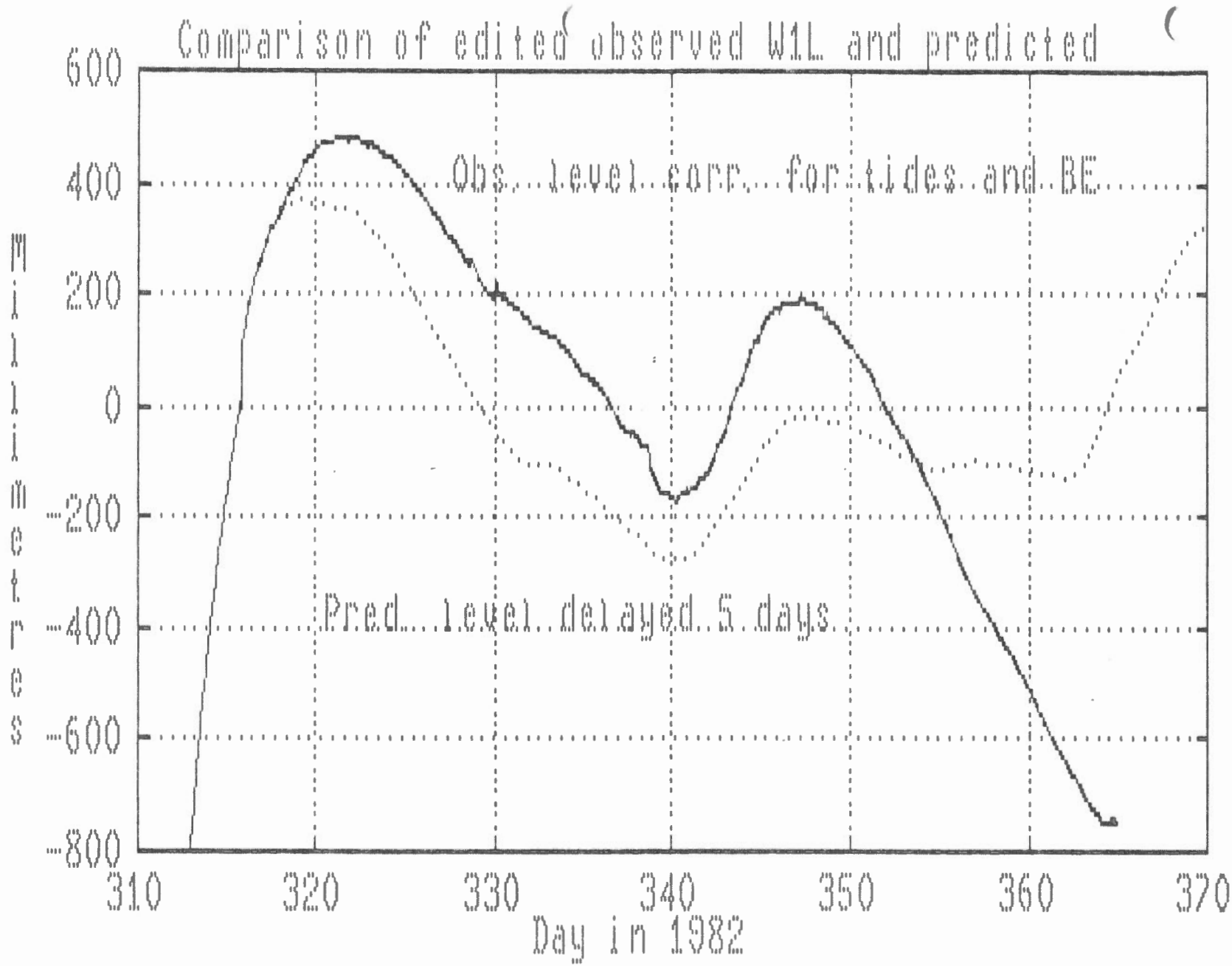
Comparison of edited observed WL and predicted
Obs. level corr. for tides and BE
Pred. level delayed 5 days
Millimeters
600
400
200
0
-200
-400
-600
-800
310
320
330
340
350
360
370
Day in 1982

FIGURE 6.5

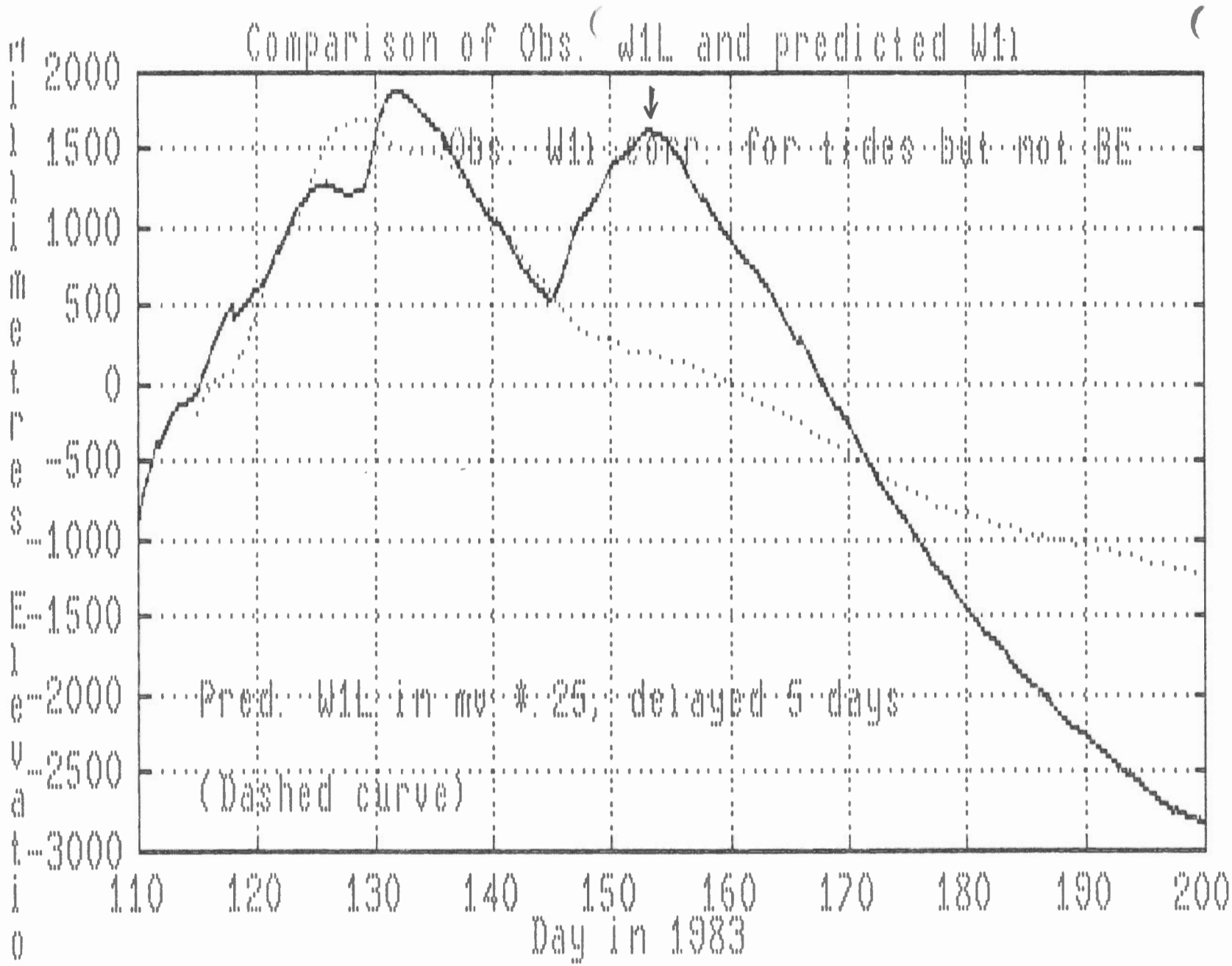
Comparison of Obs. WL and predicted WL
Millimeters Elevation
2000
1500
1000
500
0
-500
-1000
-1500
-2000
-2500
-3000
Obs. WL con. for tides but not BE
Pred. WL in mv *.25, delayed 5 days
(Dashed curve)
110
120
130
140
150
160
170
180
190
200
Day in 1983

FIGURE 6.6

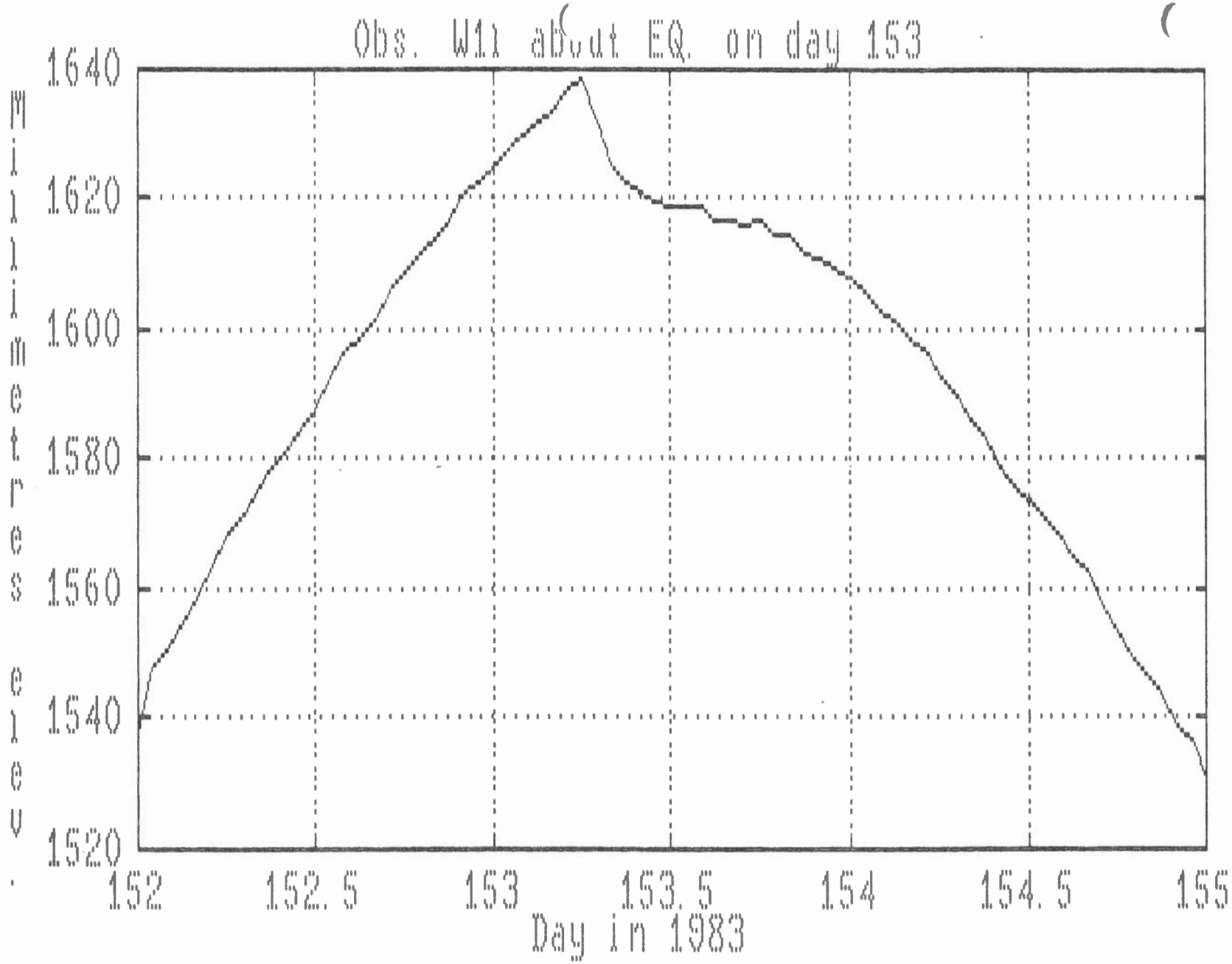
Obs. W11 about EQ. on day 153
Millimeters elev.
1640
1620
1600
1580
1560
1540
1520
152
152.5
153
153.5
154
154.5
155
Day in 1983

FIGURE 6.7

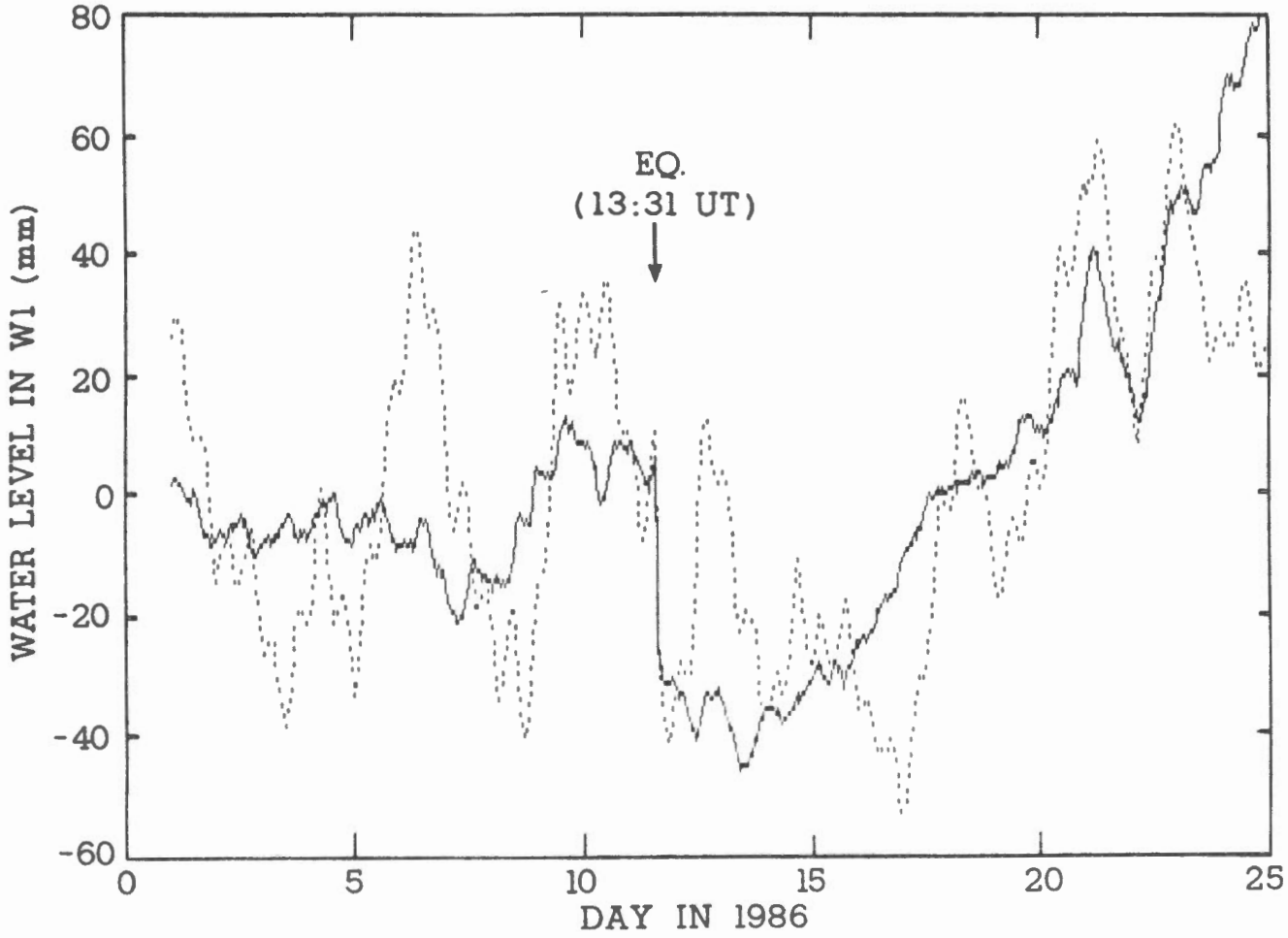
80
60
40
20
0
-20
-40
-60
WATER LEVEL IN W1 (mm)
EQ.
(13:31 UT)
0
5
10
15
20
25
DAY IN 1986

FIGURE 6.8